Methodologies, technologies and strategies for acoustic streaming based Acoustofluidics

Mercedes Stringer[1], Ziming Zeng[1], Xiaoyan Zhang[1], Yanyan Chai[1], Wen Li[1], Jikai Zhang[2], Huiling Ong[2], Dongfang Liang[3], Jing Dong[3], Yiming Li[3], Yongqing Fu[2,*] Xin Yang[1,*]

[1] Department of Electrical and Electronic Engineering, School of Engineering, Cardiff University, Cardiff CF24 3AA, UK

[2] Faculty of Engineering and Environment, Northumbria University, Newcastle Upon Tyne, Newcastle NE1 8ST, UK

[3] Department of Engineering, University of Cambridge, Cambridge, CB2 1PZ, UK

Corresponding authors: Dr. Xin Yang (YangX26@cardiff.ac.uk), Prof. Yongqing (Richard) Fu (Richard.fu@northumbria.ac.uk)

Contents

Abstract

Acoustofluidics offers contact-free manipulation of particles and fluids, enabling their uses in various life sciences, such as for biological and medical applications. Recently there have been extensive studies on acoustic streaming based acoustofluidics, which are formed inside a liquid agitated by leaky surface acoustic waves (SAWs) through applying radio-frequency signals to interdigital transducers (IDTs) on a piezoelectric substrate. This paper aims to describe acoustic streaming based acoustofluidics and provide readers with an unbiased perspective to determine which IDT structural designs and techniques are most suitable for their research. This review firstly qualitatively and quantitatively introduces underlying physics of acoustic streaming. Then it comprehensively discusses the fundamental designs of IDT technology for generating various types of acoustic streaming phenomena. Acoustic streaming related methodologies and the corresponding biomedical applications are highlighted and discussed, according to either standing surface acoustic waves or travelling surface acoustic waves generated, and also sessile droplets or continuous fluids used. Travelling SAW based acoustofluidics generate various physical phenomena including mixing, concentration, rotation, pumping, jetting, nebulization/atomization, and droplet generation, as well as mixing and concentration of liquid in a channel/chamber. Standing SAWs induces streaming for digital and continuous acoustofluidics, which can be used for mixing, sorting, and trapping in a channel/chamber. Key challenges, future developments and directions for acoustic streaming based acoustofluidics are finally discussed.

Keywords: Acoustic Streaming, Surface Acoustic Wave, Interdigital Transducer, Acoustofluidics

1. Introduction

Interactions between acoustics and fluids have been well known for thousands of years. For example, the ancient Chinese spouting bowl (or called resonance bowl) was employed spiritually for meditation to promote healing [1]. It used the vibrations generated from rubbing the handles to form standing waves which cause water droplets to be ejected above the water surface and form various fascinating patterns [2]. However, it was until year 1866 that research

on acoustic streaming was emerged when Kundt's tube experiment was designed to measure the speed of sound in a fluid [3]. By rubbing a metal rod resonator at the end of a tube in which the fluid contained small particles, these particles were periodically patterned and clustered over time at the nodes of the vibration due to the formation of standing waves [3]. Acoustic streaming was firstly reported by Dvorak in 1876 using the Kundt's tube [4]. He observed that the air was flowing from the node towards the antinodes along the axis of the tube, while the flow of the air near the wall was directed in the opposite direction [5]. This observation led to the first theoretical model derived by Rayleigh in 1884 [6], and was further studied almost a century later by various scientists including Schlichting (1932) [7] (who solved the incompressible streaming mechanisms near the wall), Westervelt (1953) [8] and Nyborg (1953) [9] (both of whom extended the methodology for a compressible fluid at its first-order perturbation).

Acoustic streaming frequently occurs in fluidics, and it generates regions of recirculation, pressure gradients, both of which can be used for particle manipulation such as patterning [10], concentration [11,12], and separation [13,14]. Particle manipulation is a widely studied topic which is related to the precise control of the dynamics of particles in biological samples. It can be realized by various passive methods, such as deterministic lateral displacement, pinched flow fractionation, crossflow filtration, hydrodynamic filtration, and inertial microfluidics [15]. Although these methods are often advantageous owing to their simplicity and low costs, they do not always offer precise and on-demand control in comparison to many active methods involving external forces or fields, such as magnetic [16], electrical (e.g., based on electrokinetic [17] effects such as free-flow electrophoresis [18] and dielectrophoresis [19]), optical [20 21], and ultrasonics or acoustic wave forces. Among these active methods, acoustic wave based ones have the advantage of manipulating various bioparticles, from nanometer-sized extracellular vesicles to micrometer-sized circulating tumor cells (CTCs), with considerable throughputs and high compatibility [22–26]. These devices are not only non-invasive, label-free, and contactless, but also convenient to be integrated with other systems for multifunctionality [25,27,28].

Acoustic streaming can also generate acoustic pressure or force to perform operations such as deformation, transportation and manipulation of bulk fluid, namely jetting [29,30], nebulization or atomization [31–34], microscale streaming [35], object rotation [36,37]. All of these have established a myriad of emerging medical applications. Figure 1 schematically illustrates examples of generation of acoustic streaming by using IDT techniques, and its methodologies and applications. A handful of popular IDT designs (bidirectional IDT, chirped IDT, slanted-finger

IDT, and focused IDT) are shown in the center. Figure 1 also include examples of acoustic streaming based acoustofluidic applications (drug delivery [38], bioprinting [39], pumping droplets [40], small organism phenotyping [36], chemical reactions [41], particle sorting/separation [11]) and their respective methodology (nebulization, jetting, transport, rotation, mixing, separation, trapping). Overall, Figure 1 displays a glimpse of the possibilities that acoustic streaming based acoustofluidics could offer. Although this phenomenon is well known and widely studied for decades, it has only recently been attracted for microfluidic applications as it overcomes a lot of challenges, which are caused by low Reynolds numbers of micro- or nanoscale liquids, either in sessile droplet format or a continuous fluid within microchannels or microchambers [42–45].

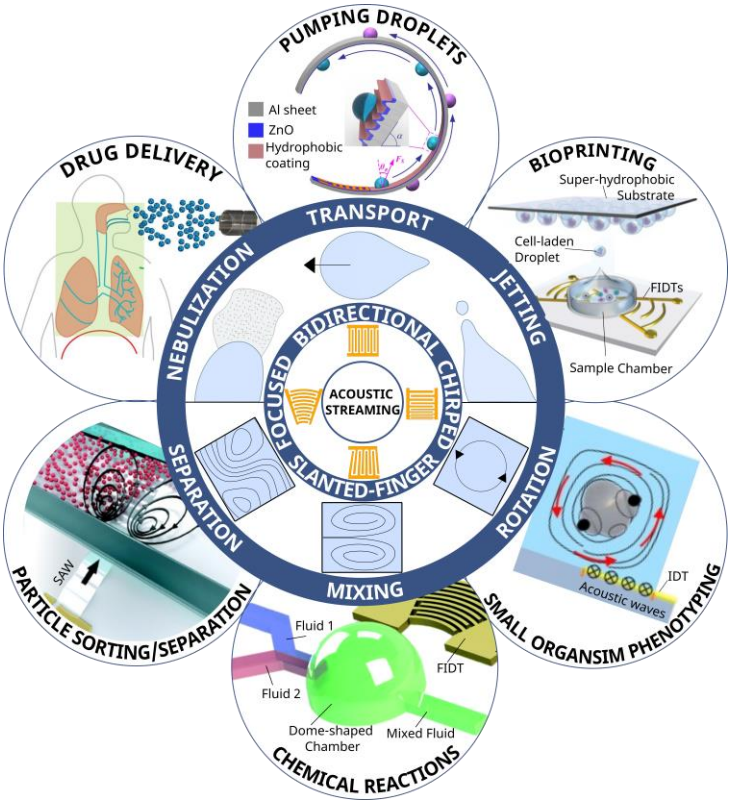

Figure 1. The generation of acoustic streaming by using IDT techniques, and its methodologies and applications. Popular IDT designs (Bidirectional IDT, Chirped IDT, Slanted-Finger IDT, and Focused IDT) are shown in the center. Example methodologies generated by IDTs (nebulization, jetting, transport, rotation, mixing, separation) are illustrated in the middle circle, and relevant acoustic streaming applications based on the respective methodology (drug delivery [38], bioprinting [39], pumping droplets [40], small organism phenotyping [36], chemical reactions [41], particle sorting/separation [11]) are should on the outer circle.

In-depth reviews of these ultrasonic or acoustic wave methods for particle manipulation and acoustofluidic functions have previously been given by many researchers [2,27,46–51]. Although these reviews have covered most critical information on fundamental mechanisms and chemical, biomedical, biological applications of acoustofluidics, acoustic sensors and lab-on-a-chip, none of them are focused on the advances in methodology and techniques based on acoustic streaming for both liquid droplets and continuous flow liquids. Therefore, this paper aims to focus on fundamental designs, techniques, and key applications of acoustic streaming, providing qualitative and quantitative discussions of its mechanisms, and highlight its key biological and medical applications (which can be revealed from Figure 1).

2. Fundamental of surface acoustic waves

Acoustic waves are generated by applying radio-frequency (RF) signals to electrodes which are commonly patterned onto a piezoelectric substrate, such as quartz or lithium niobate ($LiNbO_3$) or lithium tantalate ($LiTaO_3$). The resulted acoustic waves propagate either in the direction perpendicular to the surface of the material into the bulk medium (bulk acoustic wave or BAW), or along the surface of the material (surface acoustic wave or SAW). This review mainly discusses SAWs, whose electrodes are consisted of two metallic interlocking comb-shaped arrays called interdigital electrodes (IDEs) or interdigital transducers (IDTs), which convert electrical energy into acoustic waves through the reversed piezoelectric effect. When an RF voltage is applied to the IDTs, it causes alternating regions of tensile and compressive strains between the fingers of the electrode, thus producing mechanical waves which can propagate on the surface. IDTs have been extensively investigated in the past fifty years for usages in RF communications or filters applications [52,53], and radio-frequency identification (RFID) [52,54,55]. However, for acoustofluidic applications, this is a relatively new and an exciting area to be explored [53,56].

SAW devices can produce different types of surface wave modes to target various applications [28]. Most SAW devices are designed to generate Rayleigh waves which propagate along the surface of the substrate, with both longitudinal and vertical shear components. In Rayleigh waves, particles on the surfaces have elliptical trajectory, and show a rapid decay of particle oscillation with depth [57]. There are strong interactions of Rayleigh waves with the liquid (also the particles inside), which enable them suitable for microfluidic applications. The velocity of the waves is dependent on the material of the substrate and the orientation of the crystals. A conventional Rayleigh SAW device typically consists of an IDT to create travelling surface

acoustic waves (TSAWs) as shown in Figure 2(a). If a pair of these identical IDTs are used and placed opposite to each other, two oppositely propagating TSAWs will interfere each other, creating a standing surface acoustic wave (SSAW), illustrated in Figure 2(b). These SSAWs produce pressure nodes (PNs) and antinodes (ANs) between two IDTs, which are often used for particle manipulation [58,59].

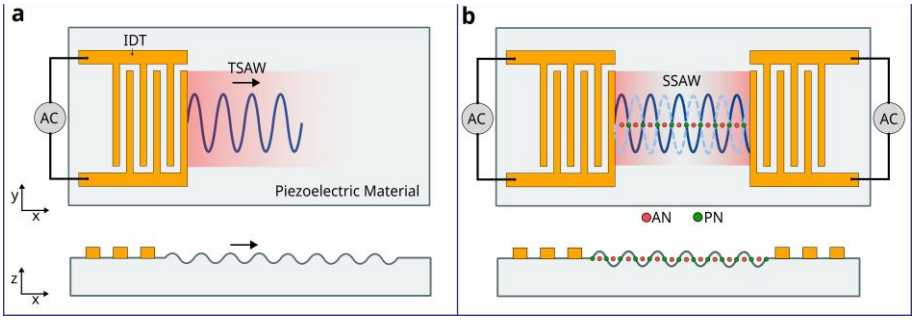

Figure 2. Schematic of the top and side views of SAWs generated by conventional IDT devices[60].**(a)** A single IDT producing TSAW. **(b)** A pair of opposite IDTs producing SSAW, demonstrating regions of PNs and ANs.

Apart from the fundamental Rayleigh waves (illustrated in Figure 3(a)), higher wave modes of SAWs in a layered SAW device are called Sezawa waves, which mainly propagate through the boundary or interlayers at a higher velocity than that at the top layer [57]. Lamb waves (Figure 3(c)), which are often generated in thin plate or membranes, are similar to Rayleigh waves. However, they travel along the whole plate structure (i.e., along both upper and lower surfaces) and hence have two free surfaces as guiding boundaries, rather than just one free surface [61]. Shear horizontal SAWs (SH-SAWs, Figure 3(b)) propagate on the substrate surface as well as on many piezoelectric thin films, all of which have in-plane crystal textures [62]. Love waves occur in SH-SAWs (Figure 3(c)) whose surface is covered with a thin wave guide layer. The SH-SAWs and Love mode waves are mainly used for biosensing rather than microfluidic applications, due to their less damping effects or weak coupling with the liquid, compared with those of the Rayleigh ones [57].

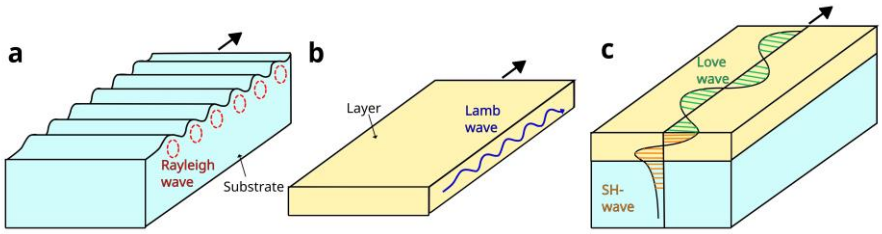

Figure 3. Illustration of types of wave propagation by means of their distribution of displacements[62]. **(a)** Rayleigh wave[63] **(b)** Lamb waves[64] **(c)** Shear horizontal waves and Love waves[57].

A typical SAW IDTs (using an SAW resonator as an example) include the electrode fingers, bus bars and electrode pad, and in many cases, the reflectors. For biosensing or medical diagnosis applications, these SAW devices are required to achieve higher SAW frequencies, larger amplitude, smaller width (higher quality factor), reduced noises, and precise IDT dimensions. SAW devices with frequencies from tens of MHz up to tens of GHz with high quality factor and low noise have been extensively reported [64–67]. Whereas for microfluidics applications, these SAW devices are required to generate multiple microfluidic functions which often require higher output powers, higher vibration amplitudes, various types of wave modes, possible wider range frequencies (e.g., from low frequency of a few MHz up to a few hundred MHz). Some high frequency SAW devices (e.g., a few hundreds of MHz) were explored for manipulating nanoscale droplet, single cells or sub-micron particles [68,69].

When designing SAW IDTs, there are different issues to be considered, e.g., geometry/thickness, electrode materials selections, mass loading, piezoelectric shorting, electrical regeneration and geometric discontinuity, strength of electromechanical constant and metallization patterns [70,71]. Recently many studies have been done on the design and patterning of various types of electrodes for lab-on-a-chip applications (including bio-samples functions and precise sensing functions), and more importantly, to improve microfluidic functions [53,56]. However, currently available IDT designs are purposely developed for RF communication or various sensing applications, and not specifically focused on their designs for the optimum acoustofluidics functions [25]. Therefore, in this paper, we will firstly introduce the mechanisms of acoustic streaming and acoustofluidics, and then discuss various IDT designs and their relevant application to acoustofluidics.

3. Mechanisms of acoustic streaming and Acoustofluidics

Acoustic streaming is a phenomenon that occurs in different forms due to its sensitivity to various geometries and boundary conditions. It is observed in Newtonian fluids, superfluid and non-Newtonian viscoelastic liquids, thus have found various applications [72]. This section aims to provide the key information about generation mechanisms of acoustic streaming and describe the fundamental theories given its ubiquitous appearance.

3.1. Governing equations and related forces

Acoustic streaming can be analyzed quantitively using fluid dynamics' well-known continuity and momentum equations, assuming the fluid is homogeneous and isotropic, i.e., [2]

$$\frac{\partial \rho}{\partial t} + \nabla \cdot (\rho \boldsymbol{v}) = 0 \tag{1a}$$

$$\rho \frac{\partial \boldsymbol{v}}{\partial t} + \rho(\boldsymbol{v} \cdot \nabla)\boldsymbol{v} = -\nabla p + \mu \nabla^2 \boldsymbol{v} + \left(\mu_\mathrm{b} + \frac{\mu}{3}\right) \nabla \nabla \cdot \boldsymbol{v} \tag{1b}$$

where $\boldsymbol{v}$ is the flow velocity, t is time, p is the pressure of a fluid, μ_b and μ are the bulk and the shear viscosities of the fluid, respectively. The bold represent vectors, and the normal are the scalars. For simplicity, all the external fields such as gravity, buoyance, and electromagnetism have not been considered. As only the isothermal case has been considered in many cases, the heat transfer equation is normally not required [73]. The left side of equation 1 is the inertia force per unit volume of fluid. The first term is the unsteady acceleration, and the second term is the convective acceleration. Convective acceleration is associated with the Reynolds stress [2]. The net forces per unit volume on the right side include pressure gradient and viscosity gradients [74]. These equations can be used with the boundary conditions and the linear relationship between pressure p and mass density ρ to predict the motion of the fluid [75].

$$p = c_0^2 \rho \tag{2}$$

where c_0 is the speed of sound in the fluid. Nevertheless, these equations are difficult to solve analytically. The only concept with a thorough foundation is perturbation theory which can only be used for slow streaming[27]. The liquid flow has two components, i.e., the fluids acoustic motion and the streaming motion. Slow streaming is generated when the velocity of the acoustic component is greater than the steaming component and only encounters resistance from viscosity [27]. It is often called linear streaming as the second-order governing differential equations in the perturbation expansion are linear, and the convective acceleration is thus disregarded. Although being called linear streaming, it should be noted that this streaming is

still caused by many nonlinear effects [76]. Whereas fast streaming is generated when the streaming velocity is in the same order or larger than the acoustic component. The nonlinear component is included such that convective acceleration needs to be considered. This paper is mostly focused on the theory of slow streaming.

Reynolds number (R_e) is a parameter used to describe the characteristics of the flow. It is the ratio of inertia to viscous terms. The flow is laminar when the viscous force dominates or turbulent when the inertia forces dominate. For slow streaming, the effect of inertia on the streaming motion is neglected by comparison to viscous effects and hence slow streaming occurs when the flow is laminar. Whereas, for fast streaming, the effect of inertia cannot be neglected hence $R_e > 1$. Reynolds number is dependent on the flow velocity and the fluid mechanical system [77]. It is defined as,

$$R_e \equiv \rho U_0 \mathcal{L}/\mu \qquad 3$$

where $\mathcal{L}$ is the characteristic length, $U_0 \equiv |\mathbf{U}|$ is the characteristic flow velocity, which includes both the velocity of the fluid $\boldsymbol{v_0}$ and the effect of the acoustic propagation $|\mathbf{U}| = \boldsymbol{v_0} + \langle \rho_1 \boldsymbol{v_1} \rangle / \rho_0$. Reynolds number for each streaming form uses a different length scale: Schlichting $\mathcal{L} = \delta_v$, Rayleigh $\mathcal{L} = \lambda$ and Eckart $\mathcal{L} = L$. δ_v is viscous penetration depth, and L is a characteristic length scale much larger than the acoustic wavelength λ [2].

R_e is usually low in most of microfluidics due to their small dimensions. The flow is usually laminar, and no turbulence occurs. Using perturbation theory, the slow streaming can be modelled in a predictable linear manner. However, R_e can become quite high in cases of fast streaming, where the flow turns more unstable, and the nonlinear term needs to be considered in the analysis [2,75].

3.1.1. Streaming Analysis with different flow velocity regimes

Perturbation theory is a method to find approximate solutions for a continuity and momentum, as shown in Eq. 3. A linearized form of these equations can be obtained by considering minor disturbances in density, pressure, and velocity;

$$p = p_0 + \varepsilon p_1 + \varepsilon p_2 + \cdots \qquad 4a$$

$$\rho = \rho_0 + \varepsilon \rho_1 + \varepsilon \rho_2 + \cdots \qquad 4b$$

$$\boldsymbol{v} = \boldsymbol{v}_0 + \varepsilon \boldsymbol{v}_1 + \varepsilon \boldsymbol{v}_2 + \cdots \qquad 4c$$

where subscripts 0, 1, and 2 represent static (absence of sound), first-order, and second-order quantities, respectively. In the absence of sound, the undisturbed state, $\boldsymbol{v_0}$, is 0 as the fluid is

quiescent. The Mach number $\varepsilon = v_1/c_0$ is used as the smallness parameter [2]. It is defined as the ratio of fluid velocity to the speed of sound. This method assumes that the successive approximations converge, hence ε is sufficiently small and can only be used for slow streaming analysis [2]. The successive approximations do not converge for fast streaming, and thus the perturbation approach cannot be used.

The continuity and momentum equations can be solved for each order component of the acoustic field by substituting the perturbation expansions. The first order acoustic field solution describes the acoustic motions in the system that contains oscillatory motion, where $\boldsymbol{v}_1$ is the acoustic velocity and p_1 is the acoustic pressure field. The first-order solutions can be substituted into second-order equations and time-averaged to find the solution for acoustic streaming, which contains both harmonic and steady components[27]. Physically, the second-order time-averaged velocity $\langle \boldsymbol{v}_2 \rangle$ is the acoustic streaming, and the second-order time-averaged pressure $\langle p_2 \rangle$ produces to the acoustic radiation force that occurs when the acoustic waves scatter on the particles, causing them to move[73].

Zarembo [78] used a different approach which overcomes the perturbation method limitation, allowing the acoustic streaming velocities to be larger than the particle velocities (e.g., in the case of fast streaming). It can be done by decomposing the dependent variables in the fluid to time-averaged streaming flow component and instantaneous first-order component. The streaming motion can be solved by substituting into the continuity and momentum equations and time averaging over the excitation period [2].

3.1.2. Forces in acoustic streaming

The forces on particles exposed to an acoustic wave are those due to direct irradiation by the acoustic field and indirect irradiation from scattering of the acoustic field from other objects [2]. Primary acoustic radiation pressure ($\boldsymbol{F}^{ARF}$) describes the force acting on a single particle in a fluid due to the SAW[27]. Whereas secondary acoustic radiation pressure is the force due to the acoustic interactions with other particles in the fluid[27]. Depending on the particle's mechanical properties, the particle moves towards the PN or AN due to the primary and secondary acoustic radiation forces [27,79].

Acoustic radiation force $\boldsymbol{F}^{ARF}$ is determined by the surface integral of the time-averaged second-order pressure p_2 and momentum flux tensor $\rho_0\langle \boldsymbol{v}_1\boldsymbol{v}_1\rangle$ at a fixed surface just beyond the oscillating sphere[80,81]. Hence, the generalized equation can be written as:

$$\boldsymbol{F}^{\mathrm{ARF}} = -\int_{\partial\Omega} \mathrm{d}a\{\langle p_2\rangle \boldsymbol{n} + \rho_0\langle(\boldsymbol{n}\cdot\boldsymbol{v}_1)\boldsymbol{v}_1\rangle\} \quad 5$$

where $\boldsymbol{n}$ is the unit normal vector of the particle surface directed into the fluid.

Overall, the particles in a fluid are exposed to the net acoustic radiation force and the SAW acoustic streaming induced Stokes drag force $\boldsymbol{F}^{\mathrm{drag}}$ [82]. The dominant force depends on the particles size. As a result, particles larger than a given threshold size will have their motion dictated by the acoustic radiation force. [27]. The size threshold is dependent on factors such as actuation frequency, acoustic contrast factor, and kinematic viscosity[83].

The Stokes drag force, $\boldsymbol{F}^{\mathrm{drag}}$, is dependent on particle size and shape, the fluid flow field, and the fluid viscosity [84]. Hence on a spherical particle of radius r, with medium viscosity η and relative velocity v, $\boldsymbol{F}^{\mathrm{drag}}$ it is given by [84,85]

$$\boldsymbol{F}^{\mathrm{drag}} = 6\pi\eta r v \quad 6$$

Compared to traditional fluid mechanics, microfluidics has a number of significant forces which would otherwise be insignificant in larger scales [2]. For a small scale, the fluid physics is dominated by surface tension and viscosity, whereas at a larger scale, body forces such as gravity are important [2]. Other particle-particle interaction forces also exist, such as *van der Waals* interactions, electrostatic interactions and hydrophobic/hydrophilic effects [86].

3.2. Fundamentals and mechanisms of acoustic streaming

Acoustic streaming is a liquid flow phenomenon generated by forces arising from the presence of a gradient in the time-averaged acoustic momentum flux in a fluid [86,87]. In a simple term, it is the fluid flow generated by the attenuation of an acoustic wave in the fluid, classified into two common types; boundary-driven streaming and bulk-driven streaming (also named Eckart streaming or quartz wind) [86].

Firstly, the acoustic wave is attenuated by the boundary interaction with the container walls, resulting in boundary-driven streaming. When an acoustic wave propagates parallel to a solid boundary, the non-slip boundary creates a high-velocity gradient perpendicular to the solid

surface. This creates a steady boundary layer vorticity, called inner boundary streaming (or Schlichting streaming) which is confined within the thin viscous boundary layer (called shear-wave layer or stokes layer) of thickness given by $\delta_v = \sqrt{2v/\omega}$, where v is the kinematic viscosity, and ω is the angular frequency of the acoustic wave [75]. The strong inner boundary streaming flow generates counter-rotating streaming vortices within the fluid, called outer boundary streaming, or Rayleigh streaming [75]. Boundary-driven streaming can appear as (1) a wave travelling down a waveguide, (2) a standing wave in a resonant chamber, or (3) a wave scattering off a solid object [75]. For example, for a standing wave, boundary streaming consists of a vortex-antivortex pair per half wavelength along the direction of acoustic propagation [86]. It typically occurs in smaller acoustofluidic channels where the characteristic length scale of the fluid chamber is less than the acoustic wavelength such that,

$$\lambda \gg h \gg \delta_v \qquad 7$$

where λ is the acoustic wavelength, h is the characteristic length scale of the fluid chamber and δ_v is the viscous penetration depth.

In comparison, bulk-driven streaming (Eckart streaming) is due to the viscous attenuation in the bulk of the fluid [86]. Stoke's Law of sound attenuation states that the dissipation rate is proportional to the square of the sound frequency [86]. The acoustic pressure amplitude decreases with distance from the acoustic source as the wave's amplitude diminishes. This energy loss causes a steady momentum flow, which generates a fluid jet in the acoustic propagation direction. Due to the pressure difference, fluid from the chamber's sides replaces the fluid propelled away by the streaming jet, resulting in a vortex-like flow [88]. It is more pronounced when the length of the fluid chamber L_E is greater than the acoustic wavelength, and hence typically occurs in larger devices [89].

$$L_E \gg \lambda \qquad 8$$

For BAW systems, the streaming is typically driven by the boundary layer streaming (i.e., Schlichting streaming and Rayleigh streaming), whereas streaming fields within SAW systems are typically driven by the velocity gradient resulting from the attenuation within the fluid (i.e., bulk driven streaming) [90]. This is because in a BAW field, the sound propagation is parallel to the edge of the fluid chamber giving rise to strong boundary effects, whilst these are lessened in a SAW field in which the sound propagates at an angle to the boundary [90]. For a droplet, when the SAW contacts the liquid, part of the SAW refracts into the liquid as a longitudinal wave at an angle known as the Rayleigh angle θ_R [27,91], given by the following equation,

$$\theta_R = \sin^{-1}\frac{v_l}{v_s} \quad 9$$

where v_s is the SAW velocity on the surface material, and v_l is the acoustic velocity in the liquid [92]. For example, a Rayleigh angle of about 22° is obtained when using a 128° Y-cut $LiNbO_3$ piezoelectric substrate at room temperature, where the SAW velocity is about 3,990 m/s, and the speed of sound in water is 1,490 m/s [27]. Whereas this value can be as large as 41° for a ZnO/Al plate SAW based device, as the SAW velocity in the aluminum substrate is about 1,835 m/s [93]. The SAW changes modes into a leaky SAW in the fluid that decays exponentially with distance from the source due to the attenuation by viscosity along its transmission through the medium [94]. This decay length is the attenuation length, α^{-1} [95]:

$$\alpha^{-1} = \frac{\rho_s v_s^2}{f\rho_l v_l} \quad 10$$

where ρ_l and ρ_s are the densities of the fluid and the solid, respectively. In contrast, SAW propagates in the liquid medium along the Rayleigh angle with a distinctly higher attenuation length, β^{-1} [87]:

$$\beta^{-1} = \frac{\rho_l v_l^3}{4\pi^2 f^2(\frac{4}{3}\mu + \mu')} \quad 11$$

where μ and μ' are the shear and bulk viscosities of the fluid, respectively.

Bulk driven acoustic streaming force is formed in the fluid due to the non-zero and temporally phase-shifted distribution of the pressure and velocity [50], [51]. Inner boundary streaming may also arise due to the transmission of shear from the substrate to the fluid, which is confined in the viscous boundary layer [96]. Consequently, this could drive outer boundary streaming in the bulk of the fluid. However, boundary layer streaming is not frequently reported in SAWs [98], and is often negligible compared to bulk streaming if the fluid container size and SAW attenuation length are much greater than the SAW wavelength [99].

The SAW induced streaming pattern varies dramatically with the shape of the confined liquid, the type of IDT configuration used, and the incident position, angle, operating frequency and power of the SAW [27]. Typical SAW streaming patterns that may occur for droplets and channels are displayed in Figure 4. Figure 4(a-c) and figure 4(d-e) illustrate streaming patterns in channels and droplets, respectively, demonstrating the varying streaming patterns with different SAW propagation positions and directions (blue arrow). Figure 4(a) and figure 4(b)

show the fluid being driven by the propagating SAWs (coming from the left of the channel, and the bottom of the channel, respectively), generating two vortex-like flows (top and bottom, and left and right, respectively). These types of streaming patterns can be used for methods such as mixing, concentration and rotation as outlined in Section 5.1.3. Figure 4(c) illustrates an example of SSAW streaming [100] in front view, revealing two vortexes. SSAW streaming applications are discussed in Section 5.2. SAW propagation. Figure 4(d) displays a droplet streaming pattern, where the SAW propagation enters from the left and forms two vortexes. Figure 4(e) demonstrates streaming when the SAW propagates laterally offset to the droplet, creating one vortex. Figure 4(f) shows SSAW propagation where four vortexes are created. As discussed in Sections 5.1.1 and 5.1.2, these types of streaming can be used for mixing, concentration, and pumping.

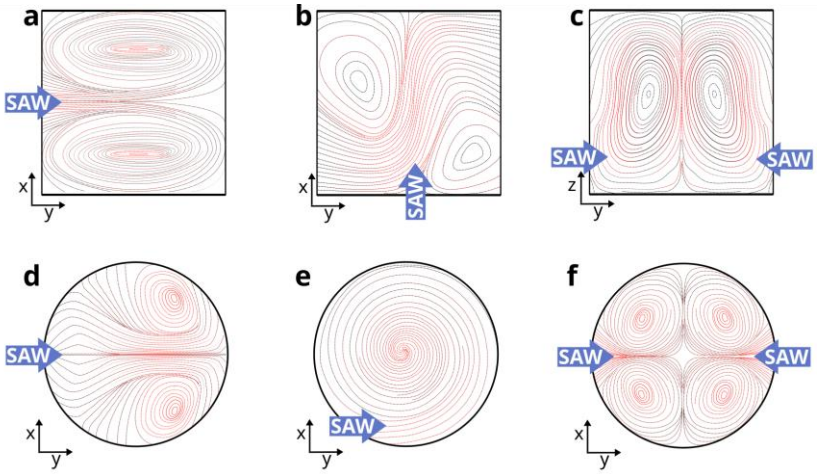

Figure 4. Illustration of two-dimensional fundamental streaming patterns for **(a-c)** channels and **(d-f)** droplets, with different SAW propagation positions as shown by the blue arrows. **(a)** and **(b)** show streaming patterns in the top view, where the SAW propagation enters from the left, and the bottom, respectively. **(c)** displays streaming patterns in the front view, where SAW propagation comes from both the left and the right producing SSAW streaming. SAW propagation enters the droplets (top view) from **(a)** the left, **(b)** laterally offset, and **(c)** both left and right (SSAW).

The input power applied to an IDT for actuating a droplet can considerably vary the streaming patterns. At low input powers (in the order of mW), preliminary acoustic streaming on the free surface is generated, which can be used for vibration, mixing and driving applications. Higher input power (e.g., above a few watts) leads to a breakup of the stabilizing interface and allows for techniques such as jetting, atomization or nebulization [101].

Two types of acoustofluidics have often been defined. The first one is called digital acoustofluidics, which is about sessile droplet under the acoustic field. Droplets act as sample carriers that can be systematically sorted, trapped, mixed, pipetted, and split. They offer many advantages such as low sample consumption, high throughput, flexible manipulation, and elimination of cross-contamination and channel fabrication [102]. Parameters including the droplet's shape, volume, contact angle and evaporation determine acoustic streaming patterns that consequently lead to variations in particles' concentration behavior [101,103].

Another acoustofluidic field is called continuous flow acoustofluidics, e.g., studying the liquid within microchannels or chambers interreacting with the acoustic waves. Channels and chambers have advantages as they often contain larger volumes of liquid, incorporate flow, and modify their boundary conditions to allow versatile applications. It is important to note that the channel/chamber boundary has a large impact on its applications. It could consist of different materials (e.g., glass capillary, polydimethylsiloxane (PDMS)), interfaces (e.g., liquid-air, liquid-glass) or geometries (e.g., different dimension/shape tubes or chambers).

For both these acoustofluidics, the methods to generate various liquid streaming in a SAW device are crucial. This can be effectively realized using IDTs and this will be introduced and discussed in detail in the next section.

4. Acoustofluidic transduction technologies for acoustic streaming and acoustofluidics

4.1. Design and manufacture of electrodes

4.1.1. Design criteria

The key design parameters for the IDTs of SAWs include: center (or resonant) frequency o_f, frequency spectrum, bandwidth, power output density, choice of electrode materials, shape/dimensions (including thickness), positions, substrate isotropic/anisotropic properties, and number of reflective electrodes [104], dispersion, substrate, reflection/transmission functions, electrode types, weighting functions, resistance, electrode length and aperture, electrode phase, electrode positions or delay effect, and wave direction or directivity (e.g., bidirectionality or unidirectionality). The main objectives for improving electrode designs include: (i) increasing the generation efficiency of acoustic waves; (ii) improving spurious signal suppressions; (iii) decreasing insertion loss; and (iv) reducing signal distortion.

Depending on the different applications (e.g., biosensing or acoustofluidics), the key issues about IDT designs are: [105]

(1) Beam divergence or wave diffraction[63]. Due to the beam steering effects, or due to the anisotropic effect of piezoelectric materials, the waves will not propagate in a direction perfectly normal to the wavefront. **Acoustic aperture**[106] (i.e., the overlapping length of electrode) needs to be designed precisely to avoid diffraction of the acoustic beam, and a narrow aperture will cause beam steering and wave spreading when propagating. IDT impedance is also dependent on this aperture. Normally it is recommended to be at least 50 times of the wavelengths to achieve an effective function.

(2) Bragg reflection[106]**.** This is the wave reflections due to the electrode interactions causing in phase scattered waves which have a much stronger reflection. This often happens when the wavelength λ is equal to the periodicity, P. This can be solved by using different electrode designs, such as double electrode (or split electrode) IDTs, which is discussed in the following section.

(3) Numbers of fingers N[63,107]. Increasing this number, the bandwidth will become narrowed, which is useful for achieving a better-quality factor of the resonant peaks. The bandwidth (equals to $2f_o/N$) is also inversely proportional to the number of fingers in the IDTs, and increasing the finger numbers can minimize spurious responses. However, too many finger numbers will cause mass loading and scattering effects from the electrodes (which might degrade the IDT's performance), as well as a much larger size or area of the electrode.

(4) Triple transit signals[106]**.** This is often caused by the output IDTs producing reflected waves, which are reflected from the opposite IDTs and then reflected second time by the input IDTs. This is also called triple-transit-interference (TTI), or the multiple path effects generated by non-matched output of IDTs as ripples with periodicity in the frequency responses.

(5) Impedance mismatch[63,108]. This is one of the key reason for the complexity of surface acoustic wave fields used for microfluidic applications [108]. The impedance matching is critical, otherwise, much of the acoustic wave energy will be dissipated within the IDTs. Electrical dissipation in other forms should be avoided, such as electrical shielding and conductive short connections. This can be solved by using a matching network or adjusting the IDT designs.

(6) Bidirectional effect[63]. A straight conventional IDT has waves propagating in two directions; thus, the wave energy will be wasted if one of the wave directions is not used. This can be resolved using different designs such as single-phase unidirectional transducer which is discussed later.

(7) Heating effect[57]. The propagating wave produces atomic vibrations that causes heating effects. Heating effects can be increased by defects, degradation, or malfunction of the device causing internal dissipations of energy, or from reflections from the power supply.

In the following sections, we will separate the IDT topics into transducer materials, fabrication techniques, and advances in IDT for acoustic streaming and acoustofluidics applications.

4.1.2. Transducer materials

IDT's materials influence the performance and electromechanical coupling coefficient of the SAW devices [109–111]. The IDTs are generally required to have a low mass to minimize wave damping. They also need to have a high acoustic impedance to confine the acoustic waves within the piezoelectric layer, and have a high conductivity to minimize the series resistance in the transmission of the excitation signals. The different electrode materials have been discussed by Fu et al. [57], based on their acoustic impedances ($Z = \rho \cdot v$, in which ρ and v are the density of material and velocity of the waves) and ξ is resistivity of the materials.

For fabricating SAW devices, Al and Au/Cr (or Au/Ti) are the most frequently used electrode materials. Al is the 3rd most abundant element on earth (after O and Si). Al electrode has its advantages of low cost, a low resistivity, and low acoustic impedance, as well as a high Q factor used as SAW IDTs, thus it is often used for delay lines and transversal filters. However, it has some critical issues such as low mechanical strength, low melting points and poor electro-corrosion resistance. Normally it requires enough thickness (commonly 100 to 200 nm) to present a low electrical resistance but should not be too thick to cause problem with mass loading effect and significantly increased acoustic impedance. Au electrodes have its advantages at high power or with liquid, or in corrosive environments. However, at higher frequency, gold IDTs show large mechanical losses, relatively large mass loading and reflection, whereas aluminum IDTs show high reflection coefficients and high Q factors at higher frequencies [112].

Some conducting and transparent oxides, such as aluminum doped zinc oxide and indium tin oxide, have also been applied as electrode materials for transparent SAW devices [113,114]. Graphene [115,116] and its derivatives, with their theoretically high conductivity and being an extremely thin and light material which would cause insignificant mass loading [117], has been

applied as the IDTs of SAW devices [118,119]. Multilayer graphene with a sheet resistance of a few tens of Ω/sq could improve the transmission properties [120].

When choosing the substrate materials to place the IDTs on, various factors should be considered, including cost, temperature dependence, attenuation, and propagation velocity. For example, the anisotropic properties of the substrates will cause significant direction-dependent electromechanical coupling effects, therefore, their orientation and cut will determine the efficiency of the device's electrical energy transduction from the SAWs. Anisotropy effect of the substrate will affect which type of waves are generated: e.g., SH-SAW, leaky SAW, or pseudo-SAW [27]. The anisotropic wave propagation velocities within the planes are critical issues for effective IDT layout designs along various crystal-cut directions [121].

$LiNbO_3$ is commonly used in SAW fabrication for acoustofluidics due to its outstanding electromechanical coupling coefficient [107]. However, due to $LiNbO_3$'s rigidity, brittleness, and anisotropic nature, many other substrates have also been explored. Piezoelectric thin films including zinc oxide (ZnO) [122–124] and aluminum nitride (AlN) can be deposited onto various substrates such as silicon (Si), glass, ceramics, diamond, quartz, glass, and more recently also polymer, metallic foils and bendable glass/silicon for making flexible devices [57,123]. Using piezoelectric films would allow for fabrication of integrated, disposable, or bendable devices. Due to the isotropic nature of thin film materials deposited onto a planar substrate, flexible designs of electrodes or IDTs, such as focused, curved, circular/annular, or randomly shaped patterns are readily achievable on thin film acoustic wave devices [57]. Additionally, bulk ceramic substrate such as $LiNbO_3$ has a low thermal conductivity and poor fracture toughness which becomes a challenge when a high power is needed. Thin films such as aluminum nitride or gallium nitride (GaN) could be a novel piezoelectric films that, although piezoelectric performance is compromised, allow for higher input power and superior thermal stability [125,126].

4.1.3. Fabrication techniques

Cleanroom manufacturing techniques involve photolithography, evaporation and sputtering, lift off or etching. These techniques allow for the fabrication of high efficiency, small-scale, precise, and reproducible IDTs. Standard patterning techniques are either subtractive or additive patterning, e.g., one method involving etching and the other lift-off, respectively. The main steps for subtractive patterning are deposition, lithography, and etching. Firstly, the wafer

is cleaned before any IDE material is deposited to ensure the metal adheres successfully. Deposition can be done by either sputtering, thermal evaporation, or chemical vapor deposition. Lithography is performed by patterning photoresist using ultraviolet light exposure through a mask to create a positive image of the IDEs after developing. Wet or dry etching can be used to etch the IDE material. Lastly, the photoresist is removed to complete the process. The additive method involves using lithography to pattern photoresist such that it creates a negative image of IDTs after being developed. The IDE material is deposited on top of the patterned photoresist. Then, the photoresist and the excess IDE material is removed using a lift-off process.

Apart from the above conventional photolithography processes, new techniques such as electron beam lithography, focused ion beam milling, or nanoimprinting, have been used for making sub-micron wavelengths, thus super-high frequency SAW devices can be obtained. For example, SAW devices with super-high frequencies (from 20 to 44 GHz) based on $LiNbO_3$, $ZnO/SiO_2/Si$, or $LiNbO_3/SiO_2/SiC$ heterostructures were reported using an e-beam lithography method [127–129].

Clean room technique however can be expensive. Brittle piezoelectric substrates such as $LiNbO_3$ are often used for making the IDTs. Not only can it be problematic to make modifications, but also it is difficult to repair any mistakes or damages once the patterns have been processed. To overcome this, IDEs can be manufactured separately from the piezoelectric material, and then pressed onto the piezoelectric substrates to generate SAWs, for example, using a printed circuit board (PCB), which is especially useful for prototyping. This method consists of mechanically clamping electrodes made using PCB or even flexible PCB with a piezoelectric substrate [130–132], thus the waves can be generated by simply applying RF frequency to the pressed IDEs on the piezoelectric substrates.

Additional methods of creating electrodes have also been explored, such as by pouring low-melting-point metal into a mold by PDMS [133], stacking aluminum foil strings onto substrate [134] and using superstrates on conventional SAW devices to allow their reusages for different applications [135]. 3D printing can be used to produce various shapes of electrodes and electrode arrays with specially designed reflectivity and directionally (e.g., bidirectionality/unidirectionality) and varied frequency spectra, although the IDTs' resolution might not be as good as those from lithography ones.

4.2. Advances of Interdigital Transducers

4.2.1. Conventional IDT structures

As mentioned in Section 4.1, the **standard bidirectional IDTs** have a simple design (as shown in Figure 5(a)), which has two electrode fingers, bus bars and electrode pad. However, it has issues such as internally mechanical edge reflections and loss of wave energy at two sides therefore half of the energy could be wasted in one direction. Various IDT designs have been studied to solve the critical issues, including straight or curved (focused or plane waves) types of IDTs, standing waves or propagating waves, and aligned or shifted waves. It should be noted that some of these IDTs are designed for sensing purposes, but not best for acoustic streaming applications.

(1) Split IDTs (Figure 5(b)). This is used to reflect some of the waves, thus reduce reflections. It is also used to minimize the spurious response due to the finger reflections.

(2) Single phase unidirectional transducer (SPUDTs, Figure 5(c)). SPUDTs have been commonly used to reflect or cancel regenerated waves using the internally tuned reflectors within the IDTs to form unidirectional SAW propagations from the IDTs. It can minimize the triple transmission effect (TTE), reduce the noise/insertion loss, and reduce the passband ripples. [136,137]. There are different designs for the SPUDTs. (1) Split finger pair by simply using 1/16 λ, in which all the gaps are equal to 1/8 λ. (2) Fixed split finger pair and varied widths to obtain a required directivity, e.g., different-width split finger SPUDT [138], in which the gap width between sections of opposite directivities as 1/16 λ and the distance between the two adjacent reflection center is ¼ λ. (3) Triple electrode section SPUDT, in which all the gaps and fingers are designed as 3λ/8, which will generate a third harmonic response stronger than its fundamental response. (4) Special designs such as with finger widths of 1/5, 2/5, 1/5, and 1/5 λ. The problems for these SPUDTs are that the small electrodes size limits the fabrication of super high frequency devices. There is a reduction in total SAW energy meaning that the SAW generation efficiency is much lower, and its insertion loss is higher.

(3) Distributed acoustic reflecting transducer (DART, Figure 5(d)). This includes a sequence of identical cells with a length equal to wavelength λ, and each cell has two electrodes width of 1/8 λ, and one electrode of width 1/4 λ, the inter-electrode space is 1/8 λ. Variable reflection can be achieved to cancel the net reflection and transmission effects. By segmenting

the reflecting electrodes, a variable reflectivity can be achieved, thus providing design flexibility. They might be beneficial for SAW microfluidics and sensors as it not only improves the performance, but also maintains the SAW devices at the best operating conditions.

(4) Floating electrode unidirectional transducers (FEUDTs, Figure 5(e)). One (or more) electrodes is/are not connected to others and are floating. In the FEUDTs, the shorted or open electrode configuration changes the transductor/reflector interaction and promote forward transmissions.

(5) Apodised IDTs (Figure 5(f)). This is achieved by varying or setting the non-uniform beam profiles for weighting a SAW transducer. In this design, the IDTs have different lengths and different positions, and they generate impulse response/pre-patterned pulse waves. The overlaps of the electrodes are varied along the length of the transducer, which can generate a specific frequency response. In apodization technique, the top electrode is designed with non-parallel edges which increases the resonant path and leads to more attenuated modes, thus degrading the strength of spurious lateral modes. This pattern is generally used for wave shaping and manipulation of frequency response of the IDTs. It can also be used for minimizing heating effects, and avoiding bulk wave interferences, diffraction, and IDT end-effects, or optimizing the output signal profile.

(6) Focused or curved IDTs (FIDT, Figure 5(g)). These IDTs can generate strong and focused acoustic force or energy, which can be used to concentrate the acoustic energy to a focal point. It has been utilized for improving pumping and mixing efficiency in acoustofluidics, and for enhancing sensitivity and resolution in sensing applications. The curved IDTs have been utilized for enhanced pumping and mixing functions with a strong concentration effect.[139] However, due to the anisotropic nature of many crystal cuts of bulk piezoelectric materials, it is recommended to modify the IDTs into a concentric elliptic shape, whose curvature might be smaller than that of the wave surface [139,140].

(7) Chirped IDTs or dispersive delay lines (Figure 5(h)). These are achieved by varying the width and frequency of IDTs to control wave modes and reflectivity, to linearly modulate the wave pitch or frequency. The bandwidth can be relatively large, and the frequency can be changed gradually by decreasing the electrode spacing and increasing the electrode spacing. It can be designed into an expander (from large width to smaller width) or a compressor (from

small width to larger width). Chirped IDTs are useful for manipulating droplets in different directions and for focused acoustic energy propagation. They are able to manipulate or change the moving direction of a droplet by changing and tuning the operating frequency continuously, thus used for manipulation of single microparticles, cells and organisms [141–143].

(8) Slanted finger IDTs or tapered or tilted IDTs (SF-IDT, Figure 5(i)). [144,145] They have varied frequencies in the IDT section by changing the electrode's periodicity. They have broad bandwidths, which can change the moving direction of a droplet by changing the operating frequency continuously [27,146,147].

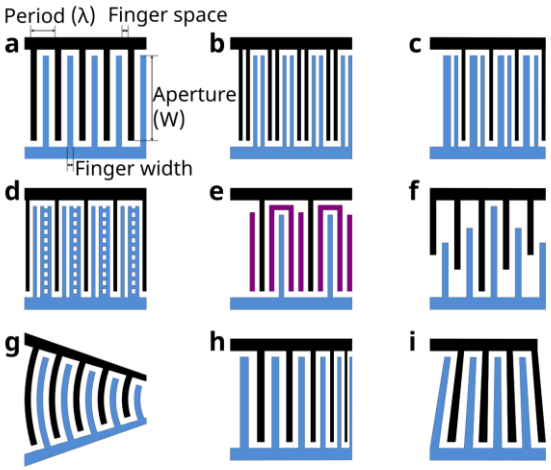

Figure 5. Conventional IDT designs. **(a)** Standard bidirectional IDTs **(b)** Split IDTs **(c)** Single phase unidirectional transducer (SPUDT) **(d)** Distributed acoustic reflecting transducer (DART) **(e)** Floating electrode unidirectional transducer (FEUDT) **(f)** Apodised IDT **(g)** Focused or curved IDT **(h)** Chirped IDT or dispersive delay lines **(i)** Slanted finger IDT or tapered or tilted IDTs (SF-IDT).

4.2.2. Unconventional IDT structures

Apart from the above commonly used IDT structures, there are many different types of uncommonly used IDT patterns.

(1) Circular or annular IDT (Figure 6(a)). Focused IDTs can be extended to create circular IDTs [148,149]. Circular IDTs have a large focused acoustic force or energy, and have been utilized for improved pumping, mixing, and jetting of droplets. However, they have the same problem

as FIDTs of the anisotropic properties of the substrates of 128°Y $LiNbO_3$ is, e.g., there is anisotropic effect for the velocities of waves along different directions. This can be improved by designing a slowness curve deviating from the circular shape, or using a concentric elliptic shape, which causes the beam direction no longer to parallel to the propagation direction [150]. Also, for these circular IDT devices, the angle dependent coupling coefficient in a device of 128°Y $LiNbO_3$ is significant. Therefore, the key issue for such a circular IDT device is to achieve uniform waves from different directions. As we mentioned before, for piezoelectric thin film based SAW devices, such an issue is often insignificant due to the isotropic wave propagation on the planar surfaces of thin film SAW devices.

(2) Dual wavelength IDTs. Two different wavelength designs in one IDT can be applied, which can generate two different SAWs after applying different frequencies. Although both IDT designs consist of the same aperture, the dual-wavelength SAWs can be generated separately or simultaneously, which can be spatially superimposed along the propagating path within the microchamber or the microfluidic channel. The generated complex acoustic pressure field can be applied to separate or mix particles of different sizes.

(3) Spiral IDT designs [151,152] or **anisotropic swirling SAWs** (see Figure 6(b) to 6(d)). These can be used to tailor acoustical vortices, or for 3-D particle manipulation and vorticity control. Spiral electrode designs can generate in-plane torsional vibrations. Spiral IDTs can be difficult to design when consider the anisotropic wave velocity in different plans and directions for many bulk piezoelectric crystals. Three types of design structures are proposed. (1) Swirling IDT designs (Figure 6(b)), which can generate varied acoustic wave fields by simply changing the applied signals; (2) Constant electrode spiral angle (Figure 6(c)), which provides a uniform spiral angle for electric field but varied intensity [13,151]; (3) Constant pitch (distance) between adjacent electrodes (Figure 6(d)), which can provide a uniform intensity of electrode fields but various spiral angles, hence this design has a better in-plane torsional displacement and vibrations than the previous one [153,154]. The last one is also called Ring waveguide resonator IDTs [155], which was reported to have a high-quality factor due to its regularity of electrode structure, and the electrical admittance does not have any sidelobes. Thus, it can be suitable for sensor applications. This design has a "slow" electrode region with a "fast" surrounding region, with the acoustic fields concentrated in the electrode region. Additionally, circular slanted finger IDTs with angularly varying finger widths and spacing can introduce frequency-

multiplexing [156]. Practically, these complex wave fields generated using spiral SAW acoustical vortices can be used for particle tweezing, liquid twisting and swirling on a single functional platform. This design can generate focused waves which are varied constantly by adjusting different focusing points in arbitrary positions [157,158]. This has been used to demonstrate for a variety of biological applications, including droplet transportation separation, fusion, and nebulization [157,158].

(4) Holographic IDTs (Figure 6(e)) [159,160]. These can be used to produce waves by designing specially metallic electrodes with equi-phase lines of the targeted wavefield at the surface of a piezoelectric substrate, showing laterally focused (cylindrical) and 3D focused (spherical) acoustical vortices. The SAW based holographic IDTs [159,160] have advantages of (i) high working frequency, allowing resolutions down to micrometric scales; (ii) easy fabrication with standard lithography techniques; and (iii) simple integration in a standard microscope since they are flat, transparent and miniaturized [159,160].

(5) Ball shaped IDTs (Figure 6(f)). The wave propagates around the equator of a large sphere in multiple roundtrips, where the number of the SAW circulations around the ball equals the SAW's propagation length. This can be used as a good sensor or acoustofluidic device on a ball-shaped device. Due to the collimation of the SAWs, the energy loss from diffraction is avoided. Therefore this is beneficial for sensors as the SAW propagation path can be much longer and the sensitivity could be higher [161].

(6) Inter-digitated IDT (IIDT, Figure 6(g)). It uses the interweaved input and output transducers to eliminate the inner transducer's bidirectional insertion losses and suppress the sidelobes of the spectrum.

(7) Tunable IDT (Figure 6(h) and multiphase IDTs (Figure 6(i)). Conventional IDTs with fixed pitch comb electrodes can be replaced by a series of densely distributed electrodes to form a tunable IDT [162]. Different wavelengths can be formed by connecting them in various configurations, without changing the electrode layout. Other tunable IDTs could be consisted of several IDTs arranged in an in-line configuration with different center frequencies and bandwidths [163].

(8) Embedded IDTs. IDTs are normally made on top of the piezoelectric substrates, which

have potential problems of reflection and scattering effects of these IDTs. One potential method to solve this is to use the IDTs fingers embedded inside the substrates [164]. However, this needs extra fabrication steps such as etching into substrates and post-polishing or other procedures [164]. This type of design is important for focused IDTs, which can minimize the finger grating effects on the angular dependence of the phase velocity [165]. For thin film-based SAW devices, this becomes easier as the IDTs can be deposited firstly onto the surface, or filling in the grooves to eliminate technological imperfections for burying electrodes [166,167].

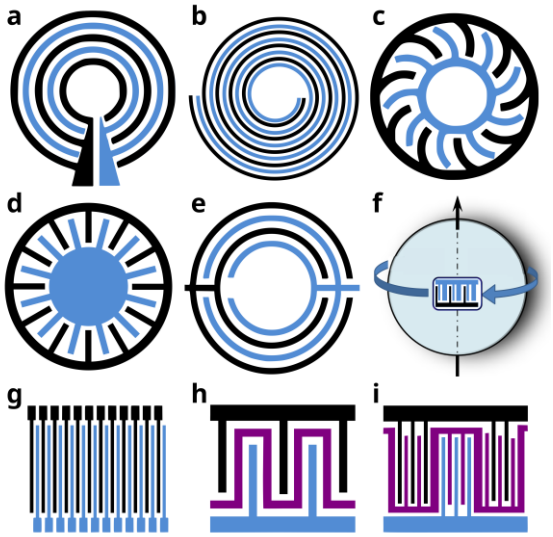

Figure 6. Unconventional IDT designs. **(a)** Circular or annular IDT **(b)** Swirling IDT **(c)** Electrode spiral angle IDT **(d)** Ring waveguide resonator IDT **(e)** Holographic IDT **(f)** Ball shaped IDT **(g)** Inter-digitated IDT (IIDT) **(h)** Tunable IDT **(i)** Multiphase IDT.

4.2.3. IDTs embedded into multi-layer structures

As explained before, due to the isotropic nature of thin film materials deposited onto a planar substrate, flexible designs of electrodes or IDTs, such as focused, curved, circular/annular, or randomly shaped patterns, are readily achievable on thin-film acoustic wave devices [121]. Due to the thin film deposition process, the IDTs do not always need to be on top of the piezoelectric materials. For example, a "liquid needle" has been the early demonstration in which a circular self-focused bulk wave acoustic transducer with circular IDTs (on both top and bottom of the thin-film piezoelectric material) are used to generate a focused acoustic wave and produce a needle-shape liquid column on the free liquid surface [168–170]. As different layers have been used

in thin-film acoustic wave devices to improve temperature stability, phase velocity and electromechanical coupling coefficient, the position of the IDTs can be designed in different ways [171]. As explained in Ref. [57], there are variations of such designs. (1) the IDTs can be on top of the substrate, and either the substrate or the intermediate layer must be piezoelectric; (2) the IDTs can be on top of the intermediate layer, and either the intermediate or the top layer must be piezoelectric; (3) the IDTs can be on the top layer, and in this case, the top layer must be piezoelectric to excite the acoustic waves. (4) two same types of IDTs on both intermediate and top layers to enhance the acoustic wave generation; (5) the IDTs can be located on top of the piezoelectric film with a short-circuiting plane underneath; (6) The IDTs can be located under the piezoelectric layer with a short-circuiting plane on top.

The IDTs can be either on the piezoelectric layer or beneath the piezoelectric layer to generate the acoustic waves. Adding a piezoelectric layer or dielectric layer with a high permittivity above the IDTs increases the electromechanical coupling, allowing the fabrication of devices with reduced insertion loss or smaller size [172]. A hard insulating top layer can shield the IDTs of the piezoelectric film or sub-layers and the substrate from harsh environments or liquids, thus enhancing the long-term stability of the devices [173].

In brief, IDT designs and fabrications are critical in generating streaming patterns using SAW devices. Different IDT designs and configurations can generate a variety of sensing functions and distinct streaming patterns. Adjusting the IDT design, configuration, and input parameters (such as applied power, amplitude and frequency) makes it possible to improve sensitivity, or manipulate the acoustic streaming patterns for the desired applications, as discussed in the next section.

5. Acoustofluidic streaming applications using transducer designs

SAW devices are increasingly used in biomedical applications as they are simple but meet most of point-of-care requirements. Numerous actuation techniques with different applications can be achieved depending on factors such as the boundary conditions (sessile droplet, open or closed channel or chamber), static liquid or flowing liquid, the power delivered to the device (ranging from mWatts to Watts) and the IDT designs (for example conventional IDT, FIDT). The following sections will discuss various applications based on travelling SAWs (TSAWs) and standing SAW (SSAWs) based acoustic streaming and acoustofluidics.

5.1. TSAWs based streaming and acoustofluidics

TSAWs generates physical phenomena of streaming driven particle behavior and the drifting of particles due to acoustic radiation forces, under propagating acoustic waves into the substrate and liquid [174]. TSAWs typically propagate in one direction [27], trigger mixing through streaming vortices, and produce shear stress on cells within a microchannel or microchamber. TSAWs have been applied more commonly to cause mixing, pumping liquids, or translocation of droplets, generating jetting and nebulization. Text for applications Figure XXX.

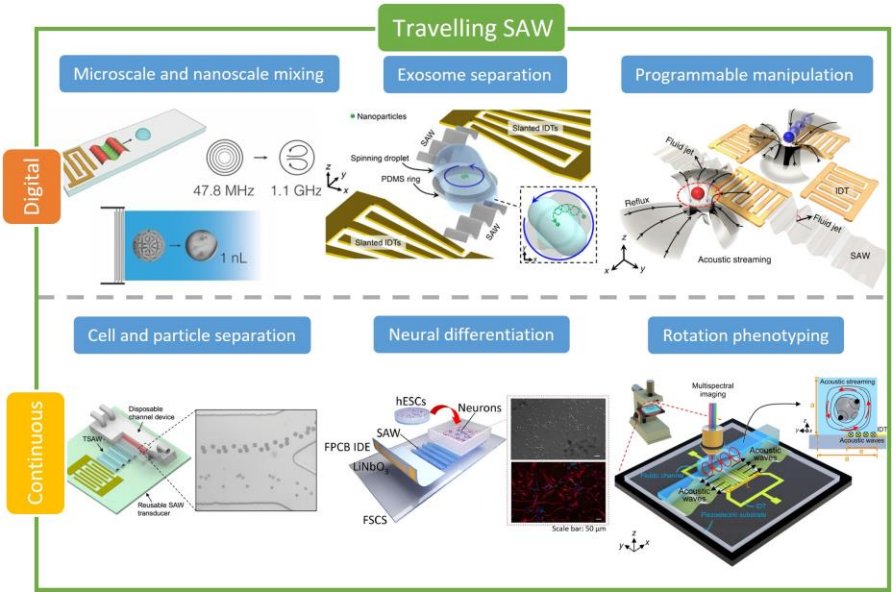

Figure X. Examples of real-life medical applications of TSAW streaming, for both digital and continuous acoustofluidics. **TSAW digital**: **(left)** A gigahertz SAW device for nanoscale droplet mixing. Reproduced with permission.[175] Copyright 2014, Wiley. **(middle)** A SAW device enabling droplet spinning and induced vortex streaming for concentration and separation of exosomes. Reproduced with permission.[14] Copyright 2021, Science. **(right)** Four IDTs (one unit/pixel) for programmable digital acoustofluidics. Reproduced with permission.[176] Copyright 2018, Nature Communications. **TSAW continuous**: **(left)** A detachable device with a reusable IDT and a disposable microchannel, for size selective PS microparticle separation. Reproduced with permission.[177] Copyright 2016, The American Chemical Society. **(middle)** A detachable FPCB device for neural differentiation of human embryonic stem cells. Reproduced with permission.[178] Copyright 2022, Elsevier. **(right)** An acoustofluidic chip for enabling rotational manipulation of zebrafish larvae for contactless morphological phenotyping. Reproduced with permission.[36] Copyright 2021, Nature Communications.

5.1.1. Mixing, concentration, and splitting of sessile droplets in digital acoustofluidics

Mixing

Microfluidic applications involving sessile droplets are hampered by diffusion-limited mixing due to their small dimensions. SAW devices can be used as a mixer to overcome this issue. It is effective to use TSAW induced streaming to mix sessile droplets [179] and nanoliter order droplets [175] by placing a singular straight IDT directly opposite to it (Figure 7(a)). This droplet mixing can be used in applications such as size tunable nanoparticle fabrication using droplet fusion [180], or particle sampling device for the collection of airborne micro-particles [181]. TSAW streaming can be utilized for cleaning biological sensors, by removing fouling caused by nonspecific binding proteins on the surface, to allow more accurate determination and reuse of the devices [182]. The TSAW induced mixing can be combined with a metal enhanced fluorescence [183] or surface plasmon resonance system [35], to improve mass transfer for biosensing capabilities. Moreover, combining a singular straight IDT device and electrowetting on dielectric (EWOD) can precisely guide and position microdroplets, for example, EWOD assisted SAW particle streaming and concentration, SAW assisted EWOD splitting, and EWOD assisted SH-SAW sensing [184]. The addition of an electric field can also increase the streaming velocity in a droplet by a factor of about 2-3 and change the flow pattern compared to that without the electric field [185].

As a result of the mixing and hence inhomogeneously acoustic streaming in a droplet, cells within the liquid droplet will experience a shear force [186]. This shear force may interact with cells through biological pathways, including the cell membrane, extracellular matrix, and cytoskeleton, instead of simply displacing cells [187]. The shear forces can induce action potentials [188] and calcium responses [189] in neurons, and affect cell adhesion and survival rate in cell culture [187,190,191]. For example, an actuated straight IDT can result in the collision between cells and magnetic Ag-nanowires in a cell droplet, leading to 97% lysis efficiency with a power of just 1 Watt [192]. Similarly, by using a 17.1 MHz electrode of width controlled SPUDT to ensure that the acoustic energy is directed solely in the forward direction, HEK 293 cells can be effectively detached and sorted from A7r5 cells based on differences in adhesion strength within minutes [193]. In Ref. [190], an FIDT has been used for characterization of adhesive properties of red blood cells (RBCs) in a 9 µm droplet within just 30 s. This method can be used to perform rapid diagnostics and disease monitoring in a small fluid volume, which is attractive as it requires no external rising agents such as trypsin, typically used for cell dissociation from the solid substrate.

When mixing particles with a high rate of mass transfer, it is necessary to consider the size of the particles. Large particles are affected mainly by radiation forces, while small particles will flow along with the vortices of acoustic streaming [194]. The uses of both the acoustic radiation force and the acoustic streaming generated by a 20 MHz straight IDT can be used simultaneously concentrate and separate two microparticle sizes (e.g., 6 and 31 μm polystyrene-PS particles [195]) in a sessile droplet. The smaller particles are dispersed in the bulk of the droplet due to drag force, whereas the larger particles are concentrated on the free surface of the droplet due to the radiation force. This demonstrates the existence of frequency-dependent crossover particle size that can affect species partitioning.

Concentration

The key for the concentration of an object within a droplet is the asymmetric distribution of SAW radiation along the width of the droplet. It is possible to achieve this by different schemes of symmetry breaking of SAW propagation to generate an azimuthal liquid recirculation as shown in Figure 7(b-d). The concentration effect can also be generated by placing the droplet along one side of the IDTs with a reflector (Figure 7(b)). Shielding off one half of an open reflector using a damp material allows control over the SAW that is reflected (Figure 7(c))[196]. Additionally, cutting the edge opposite to the input IDT at an angle to the propagation axis can effectively reflect the SAW radiation at an angle, resulting in symmetry breaking (Figure 7(d)). Using this method, it is possible to efficiently concentrate micrometer sized objects, such as PS microspheres (1 to 45 μm) and living yeast cells (10-20 μm) using low powers from 120 to 510 mW [196]. The concentration of particles can increase analyte detection sensitivity and overcomes the diffusion limitation without particle damage, allowing a range of sensor technologies.

Four distinct regimes (R1-R4) of particle concentration that are mostly available at higher frequencies can be produced by placing a singular straight IDT offset to a droplet as shown in Figure 7(e)[12]. In R1, the particles are concentrated at the center of the droplet in the form of a bead. In R2, the particles are around the periphery of the droplet in the form of a ring. In R3, at the side of the droplet, an isolated island is formed. Finally in R4, a smaller ring is formed at the center of the droplet [12]. The different regimes are due to the various forces generated (acoustic streaming-based drag force, travelling or standing SAW-based acoustic radiation force and the centrifugal force) [12]. The regimes of particle's aggregation depend on the κ-factor (defined by $\kappa = \pi d_p/\lambda_f$, where d_p is the diameter of the particle and λ_f is the wavelength of the

844 acoustic wave in the fluid), the acoustic wavefield (travelling or standing), the acoustic waves
845 attenuation length (x_s) and droplet volume where r_d is the radius of the droplet. The attenuation
846 of the sound wave in the fluid (x_f) is negligible as it attenuates at a much longer distance, and
847 hence the focus is on the rapidly attenuating SAW wave [12].

848 A focused SAW can generate concentric surface acoustic waves which have high intensity,
849 high beam width compression ratio and small localized area. Hence, the focused SAWs can be
850 used to enhance streaming force up to 480% of the conventional SAWs [197]. Circular and
851 focused SPUDT have an increased wave intensity and asymmetry of the waves, and therefore
852 they can also be effectively used to concentrate particles, which is one order of magnitude
853 faster than straight SPUDT and several orders of magnitude faster than the conventional
854 microscale devices [198]. When comparing the different SPUDT devices, the circular SPUDT has
855 been shown effective at a given input power since it can generate the largest azimuthal velocity
856 gradient within the fluid to drive particle shear migration. On the other hand, the focused
857 SPUDT (Figure 7(f)) can generate the highest mixing intensity due to the focused SAW
858 radiation that substantially enhances acoustic streaming in the fluid [199].

859 **Separation**

860 Another method for asymmetric actuation is to use an SF-IDT, which causes a circular rotation
861 motion inducing acoustic streaming of the cells in the droplet for their separation (Figure 7(g)).
862 Such actuation has been reported to separate malaria-infected RBC at the periphery of the
863 droplet, based on the difference in cells' densities using SAWs [200]. Most acoustofluidic systems
864 that aim for nanoscale manipulation are difficult to achieve this function due to the insufficient
865 acoustic radiation force and abundance of acoustic streaming to control nanosized particles.
866 Nonetheless, this acoustic centrifuge motion can overcome such limitations. Gu *et al.* [14]
867 reported the use a pair of SF-IDTs and a circular PDMS containment ring to define the droplets
868 equilibrium shape. The SF-IDTs allows various frequencies to be applied, generating SAWs at
869 different positions on the piezoelectric substrate, and therefore spin can be created on altered
870 size droplets, so long as the wave enters the droplet from a position which has a slight bias
871 from its center line. By adding two spinning droplets with a microchannel for particle passage,
872 differential phenomena including concentration and separation can occur. Using this method,
873 exosome separation and transport can be achieved, where the right-side droplet contained a
874 greater distribution of the smaller nanoparticles and the left-side droplet with the larger

nanoparticles [14]. This configuration has also been used to perform both drug loading and exosome encapsulation [201].

An omnidirectional spiral SAW that uses a 152° Y-rotated, can rapidly rotate a microliter droplet for multi-size particles for their separations and extractions, as illustrated in Figure 7(h). The rapid rotation is realized through the axisymmetric omnidirectional spiral SAW. Separation and extraction of RBCs and platelets within mouse blood can be achieved with 83% and 97% purity, respectively [13]. Unlike previous configurations to separate particles, this method can successfully extract target particles for bio-sampling functions.

Splitting

Instead of particle concentration and separation of objects in a droplet, SAW can aid in merging and splitting of droplets as illustrated in Figure 7(i). Two single phase transducer (SPTs) [202] can realize this separation function. An SF-IDT [203] was also used for separation of water from an oil/water mixed drop. A pair of IDTs which were laterally offset modulated SAWs enabled droplets with volumes of 0.5 to 6 µl to be symmetrically divided into two equal size droplets [204].

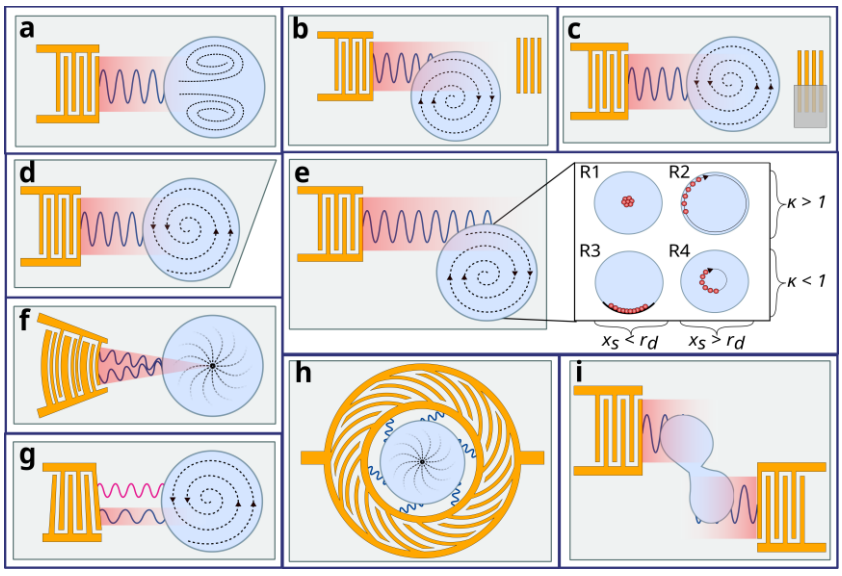

Figure 7. Droplet mixing, concentration and splitting of sessile droplets in digital acoustofluidics IDT device examples. **(a)** Singular straight IDT directly opposite droplet for TSAW mixing. **(b-d)** Schemes of symmetry breaking for rotational motion such as using a **(b)** reflector, **(c)** shielding off one half of an open reflector, **(d)** or cutting the substrate edge. **(e)**

Commented [MSM1]: If new figures stay where they are - update these and in text !!

Singular offset IDT with 4 regimes of concentration (R1) particles are concentrated at the center of the droplet, (R2) around the periphery of the droplet, (R3) at the side of the droplet, and (R4) close to the center of the droplet. **(f)** Focused SPUDT with focused SAW around center of the droplet. **(g)** SF-IDT with SAW generated at defined position asymmetrically with respect to droplet for rotation motion. **(h)** Omnidirectional Spiral IDT with circular streamlines in the droplet [13] **(i)** Pair of laterally offset straight IDTs for droplet splitting.

5.1.2. Pumping, jetting, nebulization/atomization, and droplet generation in digital acoustofluidics

Transportation

Discrete liquid pumping (i.e., droplet translation) can be achieved by applying SAW to a sessile droplet. If the applied SAW power is higher than a limit, the internal streaming leads to a deformation of the droplet, which eventually translates the droplet in the direction of the SAW propagation. The applied SAW power overcomes the forces stimulated by contact line pinning and contact angle hysteresis. For microfluidic applications, pumping of a sessile droplet in the scale of microliter without evaporation is challenging, hence low powers need to be used, or the droplet has to be encapsulated in oil [205]. Other methods to avoid problems of droplet evaporation and temperature for biological activity can be accomplished by aid of a steel ball medium [206], avoiding direct radiation of SAWs on the piezoelectric substrate using a superstrate idea, or by converting the microdroplets into a continuous flow [207].

When using a 20 MHz straight IDT SAW device (Figure 8(a)), the maximum droplet velocity happens when the diameter of droplet is equal to the attenuation length [208]. For smaller diameters of droplet, the whole SAW energy is not absorbed by the droplet. However, droplets with larger diameters move slower because the same amount of applied SAW energy was used to move a higher mass.

If the droplet viscosity becomes larger, the pumping velocity significantly decreases for small droplets (from 2 to 20 µl) [209]. The necessary power to deform and move a sessile droplet could be reduced between 50 to 75% through vibrating the droplet. This approach is important for cases for which temperature needs to be kept a constant. Another method to decrease the acoustic power required to transport a droplet is using SAW inertia-capillary modes of oscillation. For example a 19.5 MHz straight IDT can be used with Rayleigh-Lamb inertia-capillary modes to move a droplet at a speed of 5 mm/s with the required power reduced by a factor of 3 [210].

Surface properties can affect the droplet pumping velocity with SAWs. A superhydrophobic surface would minimize the contact area between liquid and solid and reduce the pinning force, making the surface slippery. However, this minimized interaction area limits the amount of the energy which can be transferred by the SAW to the liquid medium. Droplets with lower volumes at higher applied RF voltages are transported with higher velocity on hydrophobically treated surfaces [211]. Pumping of droplets with volumes up to 10 µl can be achieved using a straight IDT on a thin-film piezoelectric material treated with a hydrophobic self-assembled monolayer of octadecyl trichlorosilane (OTS) [211]. A slippery layer of lubricating oil-filled hydrophobic surface can also be used, and the threshold power to pump the droplet on a ZnO/Si SAW device can be significantly reduced (up to 85%) [212]. The surface behavior of droplet manipulation in microfluidics is discussed in detail by Wu *et al* [213].

Droplet acoustofluidic devices typically need a flat surface to operate correctly. However, changing the surface treatment and using thin-film SAW devices, such as ZnO/Si, ZnO/glass, AlN/Si [214] or ZnO/Al, can achieve droplet transportation across a wide range of substrates and their geometries, including inclined, curved, vertical, inverted, and lateral positioned surfaces[40] (Figure 8(b)).

Transporting droplets across different piezoelectric substrates could be helpful if each separate substrate has a different function, such as mixing and separating, rather than a substrate with all the operating units. For example, it is possible to use three 128° Y-X $LiNbO_3$ substrates each with their own 27.5 MHz IDT and reflector, where one is an interface chip and two are working chips 1 and 2 [216]. The interface chip can be adjusted to be the same height as working chip 2 with a gap as small as possible so that the SAW can transport the droplet across. Similarly, the droplet can be transported to working chip 1 by adjusting the height. It should be noted that although many of these methods for droplet translation do not use a FIDT, if a droplet is placed on the focal distance of an 13 MHz FIDT, it can move approximately five times faster than a straight IDT when compared to a straight IDT of the same frequency and dimension [217].

Small-scale programmable microfluidic processing can be accomplished by using SAW streaming to actuate and transport droplets along predetermined trajectories. Chemical modifications of the chip surface can be used to design the paths to create virtual wells and tubes (hydrophilic and hydrophobic regions) which confine small droplets. Depending on the actual layout of the chip/IDTs, the droplets can be split into smaller ones, merged, mixed, and

processed [218]. Instead of predetermined trajectories, acoustic streaming induced hydrodynamic traps can be used for contactless droplet transport and manipulation of droplets within volumes between 1 nL to 100 µL along any planar axis. For example, using four straight IDTs to create an 8 by 8 array (Figure 8(c)), the streaming effect pushes fluid out along one direction, and pumps the fluid (with fluorinated oil as carrier layer) along the vertical directions [176]. The acoustic streamlines converge at two horizontal stagnation points above the two symmetric sides of the IDT, hence the water droplets floating on the oil can be trapped [219]. The re-programmable digital multi-path platform can achieve various droplet manipulation (transport, merge, mix and split) and can be scaled to perform massive interaction matrices within a single device.

IDT arrays inside a layer of oil can generate acoustic streaming vortices for rewritable digital acoustofluidics, contact-free routing and active/passive gating [45]. Droplets over the transducer are guided to the center hydrodynamic equilibrium position between barrel-like acoustic streaming vortices. The vortices are extended to the adjacent transducers when multiple transducers are sequentially activated using multi-toned electrical signals. Hence a long virtual channel for unidirectional transportation and gating can be produced [45]. These programmable microfluidic processing techniques offer basic functional units that mimic electronic functionality for biomedical and biochemical applications such as on-chip bioassays, high throughput compound screening, biochemical synthesis, and droplet processing strategies that follow digital logic rules [45].

Jetting

Jetting can be generated by concentrating the wave energy into a small, focused area and maximize the mechanical displacements into sessile droplet. A nozzleless method to jet liquid can be beneficial in 2D and 3D bioprinting, needle-free fluid injection or single-molecule detection. It offers the advantages of being low cost, simple manufacturing, and the ability for miniaturization. Jetting can be achieved with a standard SAW devices such as on a substrate of 128° Y-X $LiNbO_3$ (Figure 8(d)) surface-treated with hydrophobic layer, so long as the SAW streaming force is large and strong enough to expel a droplet from the substrate [104]. Jetting can even be generated along inclined or bent surfaces using thin-film materials such as AlN/Si Rayleigh SAW device [214].

With a single IDT, the droplet is generally ejected along the Rayleigh angle (e.g., 23° on a 128° Y-X $LiNbO_3$ substrate) in the SAW propagation direction. Vertical jetting phenomena can be

generated from an SH-SAW device with a single straight IDT made on a 36° Y-X $LiTaO_3$ substrate, which is drastically different from those from the conventional Rayleigh SAWs [220,221]. The SH-SAW propagates with a relatively shallow energy penetration into the droplet. The energy and pressure are distributed randomly between the droplet and the surface in the whole contact area. The wave energy/pressure is mainly concentrated at the center of the droplet and vertically dissipated, causing vertical jetting [221].

Focused IDTs can generate increased concentration for droplet jetting and ejecting applications [29], which can be significantly affected by the substrate's wettability [121]. A pair of FIDTs can extend a pendulous droplet to form a liquid bridge with a second substrate underneath it. This straightforward method makes it possible to build capillary bridges for the low viscosity liquids, such as water, to investigate their capillary-thinning behavior [222].

Single droplets can be ejected into the air by also using a pair FIDTs (Figure 8(e)), where the droplet size can be adjusted by the pulse width duration, and on-demand repetitive droplet ejection can be managed by continuously resupplying a parent drop reservoir [223]. Such device can also be used to enable the encapsulation of single CTCs [224–226] and rare cryopreserved cells [227], as well as an acoustic droplet-based printing of tumor organoids [39] and tumor microenvironment [228]. Acoustic single-cell printing provides the ability to study cell heterogeneity toward the development of personalized cancer medicine and predicting the responses of tumors to therapy [39]. Such a nozzle-free, contact-free, and low cell-damage method will surely advance the bioprinting technology. However, it should be noted that there is a significant temperature increase of an FIDT device in water, and thus issues about high-temperature sensitivity of biological tissues and cells should be considered [229]. Single straight IDTs can also be patterned on the underside of a chip and generate surface reflected bulk waves (SRBWs) on a hybrid resonant acoustic (HYDRA) platform (Figure 8(f)) [230]. This specially designed droplet ejecting method can protect the device as the liquid does not need to contact directly with the IDT or piezoelectric substrate [231], and thus enables a modular and reconfigurable platform with individual chips in a 96 well plate.

Focused SAWs induced jetting can be easily generated using the annular pattern IDTs (Figure 8(g)). For example, a sample reservoir on top of a piezoelectric substrate with an AIDT can form picolitre (24 pL) droplets within 10 ms and encapsulate a single cells [232]. Multiple AIDTs can be combined to create a 4×4 two-dimensional ejector array which can generate drop-on-demand and continuous mode of operation 28 μm diameter droplets [233]. This open pool and

nozzleless reservoir means that droplet directionality is easily controllable with reliable ejection outcomes. Nevertheless, as mentioned previously, due to the significant anisotropic effect of such piezoelectric materials, unique designs are needed to correct the differences in acoustic velocities for an efficient or focused effect, leading to more complex modelling and mask designs [234].

Thin-film SAW devices such as using ZnO or AlN [235] not only have isotropic wave velocities but offer higher power handling capability. In-plane isotropic ZnO/Si circular SAW with an AIDT can produce vertical droplet jetting. Compared with 128° Y-X $LiNbO_3$ AIDT, ZnO annular SAW shows controllable, concentrated, thin liquid generated, whereas $LiNbO_3$ does not result in a highly concentrated thin liquid column [30]. However, the electro-mechanical coupling coefficient of ZnO SAW device is much lower than that of 128° Y-X $LiNbO_3$, thus the jetting could be relatively weak [236]. The jetting efficiency can be improved by introducing an ultra-smooth nanocrystalline diamond (UNCD) interlayer to a ZnO/Si device [237], which can help to increase the amount of the SAW energy transferred from the solid surface to the liquid medium.

Nebulization

Atomization and nebulization are methods to generate fine aerosol droplets important for numerous applications where small, similar-sized droplets are needed, such as spray cooling, inhalation therapy for drug delivery, mass spectrometry and bioprinting. Compared to other methods, they can generate monodispersed microdroplets with minimal shear and cavitation, preventing biomolecule damage due to their high frequencies and low powers. Nebulization can be carried out directly from the substrate using a single IDT (Figure 8(h)) [238–241]. For example, such a device has been demonstrated to nebulize epidermal growth factor receptor monoclonal antibodies into a fine aerosol mist for pulmonary delivery, which is beneficial for lung cancer treatment [32]. Moreover, a single IDT can use a SRBWs to achieve higher output, greater efficiency and efficacy. This type of wave propagates along and through the substrate, therefore it can draw the solution from a vial through the needle in contact with the substrate, and then nebulize the liquid [242]. Therefore *in vitro* pulmonary delivery of antibiotic alternatives can be successfully achieved against Staphylococcus aureus [38] as well as in vivo human lung deposition [242].

The droplet size of mist generated by atomization can be controlled by adjusting the physical properties of the liquid and the input power to the device [32]. For example, thin-film liquid

geometries can lead to smaller droplets and higher atomization rates, mainly due to the higher frequency used and much concentrated effects on the surfaces [31]. A thin graphene film deposited on 128° Y-X $LiNbO_3$ combined with an focused SPUDT can have up to 55% enhancement in the rate of fluid atomization [243]. Based on a comparison of SAW atomization for spray cooling with a focused SPUDT versus a SF-IDT, the focused SPUDT achieves higher efficiency. However, the SF-IDT allows placement of atomization at a specific location within the SAW device (Figure 8(i)) [244]. By using a pair of FIDTs on a ZnO/Si device with a relatively large arc angle (90°) of the IDT, it is possible to achieve an increased nebulization rate, reduced critical powers required to initialize nebulization, and concentration of the nebulized plume into a narrower size of spray [34].

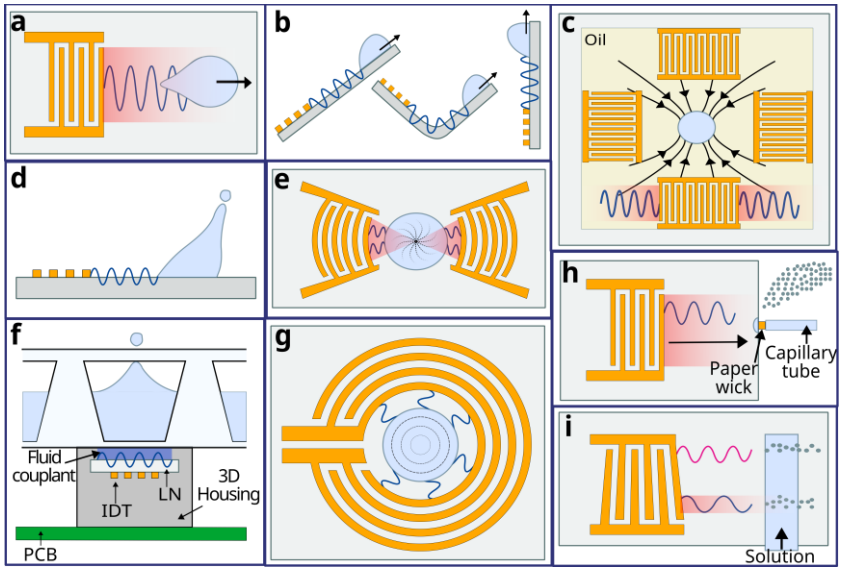

Figure 8. Pumping, jetting and nebulization for digital acoustofluidics IDT device examples. **(a)** Singular straight IDT on a horizontal surface and **(b)** inclined, curved, vertical, inverted and lateral surface for TSAW droplet transport [40]. **(c)** One unit consisting of a four straight IDT array (one pixel) for digital microfluidics [176]. **(d)** Singular straight IDT and **(e)** pair of FIDT for TSAW droplet jetting. **(f)** Singular Straight IDT on the underside of a chip for SRBW HYDRA Platform droplet ejecting [230]. **(g)** An annular IDT for TSAW droplet jetting [232]. **(h)** Singular straight IDT and **(i)** SF-IDT for TSAW nebulization.

5.1.3. Mixing, concentration, and rotation of liquid in chamber/channel for continuous acoustofluidics

Mixing

When mixing in a microchannel or a chamber, it is convenient to use a straight IDT to overcome diffusion limitations in the microscale liquid. It can support nanoparticle production [245] or increase reaction yield in the microchannel for biosensing applications [246]. When this configuration is combined with a surface plasmon resonance microfluidic sensor, SAW mixing can aid in alternative applications such as surface chemical and biochemical functionalization by improving functionalization efficiency up to 5 times with respect to that without using SAWs [247]. The key parameters to control acoustic mixing in microchannels are the SAW power, flow rate and fluid viscosity [245,248]. A SAW device with a thick PDMS channel can lead to acoustic wave attenuation and hence much SAW power could be lost. A single IDT can also be used directly underneath a PDMS microchannel to generate strong acoustic streaming for fluid mixing, and using this method, a total flow rate of 50 µl/min at a low power consumption (e.g., 12 V_{pp}) can be achieved [249]. To control mixing speed and flow patterns, an SF-IDT was used to optimize SAW amplitude and frequency due to the narrow SAW beam and variable launching point [144,250,251].

When comparing FIDTs with the straight IDTs, the focused acoustic radiation creates a high acoustic wave intensity that enhances mixing performance in a specific microchannel region (Figure 9(a)) [252]. For example, a 100.4 MHz single FIDT device can apply considerable pressure to a small region that can be focused on a water droplet on an ultrasonic couplet between a SAW device and a cell culture dish, which can facilitate the local removal of cells from a culture surface [42]. A singular FIDT can be used with a dome-shaped chamber, and can achieve mixing ratio higher than 0.9 at a total flow rate of 300 µl/min at 20 V [41]. The chamber acts as a more stabilized droplet that maximizes the effect of SAW transmitted at a refraction angle of roughly 22° with a contact angle of 68°.

To enhance mixing, one could consider the addition of bubbles in the channel [253–257]. If trapped air bubbles are excited by acoustic waves at their resonance frequency, acoustic streaming is induced and improves the fluid mixing by disrupting the laminar flow. For example, this method can mix highly viscous fluids within 50 milliseconds[255]. Nevertheless, there are concerns of bubble instability, heat generation, and inconvenient bubble trapping processes; hence other methods to enhance streaming based mixing should be considered. The geometry of the channel plays a crucial role in acoustic streaming vortices and mixing. For example, using a sharp edge [258–267] generates a large Reynolds body force when compared to non-sharp edges [258], which has proven effective in mixing[265], cell lysis [268], pumping [269] and rotation [270,271]. Such acoustic streaming enhancement is not limited to sharp edges, other microstructures[272,273]

can be used such as microcylinders[274–276], micro square pillars[277], and micro parallelepipeds[273,278].

The mixing efficiency could also be improved using three-dimensional dual SAWs generated from two focused SPUDT devices. Each of them was patterned on a piezoelectric substrate, thus achieving 100% mixing efficiency at a flow rate of 50 µl/min for 14 V or 95.6% efficiency at a flow rate of 120 µl/min for 18 V [279]. Hence, two focused acoustic waves were introduced from the top and bottom substrates in diagonally opposite directions, and induced micro swirling with the same rotational direction, which enhanced mixing performance [279]. It should be noted that although the techniques mentioned above contain the typical solid metal electrodes, other materials such as a conductive liquid-based FIDT can be used, which achieved a mixing efficiency higher than 90% at a flow rate lower than 120 µL/min and 21 V [280].

SAW can induce vibrational mixing by using SAW devices with high frequencies and lower continuous powers, compared to lower frequencies or with short but very intense pulses. Low frequencies have longer attenuation path lengths that can produce strong reflections, hence creating dominant SSAWs that suppresses the acoustic streaming. Unlike using short but very intense pulses, using low power by continuous signals is beneficial for applications which need mechanical stimulations, yet ensure that both cavitation and heating are negligible. For example, low power and single 100 MHz SAW device was used for vibration enhanced cell growth [281]. A 20 MHz device was used for accelerated neural differentiation of human embryonic stem cells [178]. Another 30 MHz FIDT device at 20% duty cycle was used to trigger intracellular calcium responses in HEK293T [282]. Due to the absence of cavitation generated at such a low power and high frequency, the 30 MHz focused SPUDT can effectively enhance the uptake of difficult-to-transfect nonadherent cell lines such as suspension T cells in just 10 min of exposure while maintaining high cell viabilities (>91%). This is much better if compared to other methods such as conventional nucleofection of 76%, which is one of the most widely used intracellular delivery methods [283].

Concentration and separation

Concentration of particles and cells within a channel and then separation have been typically realized using acoustic radiation forces [102] with SSAWs, where the objects migrate toward minimum PNs or ANs. This methods allows for concentrating and separating extracellular vesicles [284 285] and CTCs [286 287]. Nevertheless, there was also reports that a single IDT with a designed frequency of 49.5 MHz can be used to generate TSAW for separation of 10 and 25

um particles in a microchannel [177]. A combination of acoustic radiation force and acoustic streaming force can also be realized in multi-stage acoustic devices (Figure 9(b)). For example, Wang *et al.* uses a pair of straight IDTs to generate SSAW to focus CTCs and RBCs at the pressure nodes without the requirement of the sheath flow, and the pulsed focused TSAW uses acoustic streaming to push the CTCs away from RBC for CTC isolation [288]. If a pair of opposing straight IDTs are of different frequencies, two counterpropagating decaying TSAWs would be produced which can be used for particle sorting. This method allows a much longer-range force field, in which migration takes place across multiple wavelengths, and causes particles to be gathered together in a single trapping site [289].

Large amplitude and high frequency FSAWs cause strong acoustic streaming to generate fluid streamlines and vortices. This allows for functions such as size selective aggregation down to 300 nm in a closed channel [290], selective capture of 2 μm particles from mixing suspension of 1 μm particles in a continuous flow [291], and constant differential focusing of nanometer particles in a continuous channel (see Figure 9(c)) [11]. This configuration can be combined with hybrid microfluidic cell sorting techniques such as using a reverse wavy [292] or spiral [287] microchannel for passive inertial cell enrichment and as well as active TSAW single cell sorting. It could be a promising solution for practical biomedical applications as it provides high throughput and high accuracy isolation of rare cell populations.

Rotation

The same approach, by which IDTs can generate an acoustic streaming vortex in a channel, enables contactless rotation of small veritable models [37,270]. Such rotational tweezing enables high-speed, 3D multispectral imaging and digital reconstruction, which yields accurate 3D models for quantitative evaluation of morphological characteristics and advanced combinations metrics useful for small organism phenotyping, screening, and microsurgery. For example, rotation of Caenorhabditis elegans can be achieved by simply using a pair of straight IDTs with a frequency 19.32 MHz and activating one at a time to create a single vortex and hence rotate along the corresponding acoustic streaming direction [37]. However, the vortex size is limited and insufficient to rotate large organisms in the millimeter scale. Rotating larger organisms, such as zebrafish larvae are commonly used in rapid drug screening and disease evaluation, hence it is vital to develop functional platforms for clear visualization and accurate analysis for high throughput phenotypic evaluations. Quantification and 3D reconstruction can be achieved by rotating the zebrafish larvae using a straight IDT and a patterned fluidic channel

aligned on and parallel to the lateral side of the IDT with half of its width on the IDT [36] (Figure 9(d)). The fluid above the IDT forms a strong, stable, and consistent single unidirectional vortex pattern [36].

The designed rotation mechanism can be used to manipulate and drive objects, such as a centrifugal microfluidic platform. For example, a miniaturized lab-on-a-disc (miniLOAD) SAW device with two offset FIDTs was reported in Ref. [293]. The acoustic streaming drove the rotation of thin millimeter discs atop of a fluid coupling layer, on which microchannels was fabricated so that operations can be achieved. By adding a second pair of opposing offset FIDTs, the rotational velocity and direction of the disc can be controlled by altering the input frequency to the transducer [294]. Moreover, a pair of opposite SF-IDTs can be used for the miniLOAD device to alter the frequency when a disc of a different size needs to be used (Figure 9(e)) [294].

Compared to these large-scale structures, precise rotation and manipulation of microparticles in a channel need precisely controlled. For example, using six IDTs (divided into two sets) and symmetrically distributed around an annular shaped changer at an angle of 120° can lead to tri-directional symmetrical acoustic tweezer [295] as shown in Figure 9(f). Here the TSAWs are generated to precisely control microparticle movements which allows programmable motion control by switching the excitation combinations of IDTs, producing linear, clockwise, and anticlockwise trajectories. An array of IDTs, designed in relation to the anisotropic properties of the substrate, can also produce similar swirling acoustic vortices for fluid actuation and particle manipulation [158]. Similarly, an array of piezoelectric transducer plates can produce stable, symmetric pairs of vortices to create hydrodynamic traps for object manipulation[296]. In fact, acoustic tweezers can be achieved without a complex transducer array yet manipulate a wide range of particle sizes. With a single transducer, the acoustic radiation force in two dimensions is combined with an acoustic streaming vortex for levitation in the third dimension[297].

Droplet manipulation

Fluid in a droplet form in another liquid within a microchannel can be controlled through acoustic streaming. For example, an SF-IDT in an H-shaped junction for the regulated flow switching between two fluid streams [43]. Likewise, liquid droplets in a microchannel can be precisely controlled for applications such as isolated microenvironments without cross-contamination [298]. It was reported that droplets can be selectively merged using an SF-IDT to

trigger the biochemical reactions [299] [298], encapsulate samples [300], or using an FIDT to selectively dispense based on their volumes [301]. Nanoslit channels have also been created and combined with the TSAW streaming to perform notoriously difficult nanoscale manipulation due to the dominance of surface and viscous forces [302,303]. Using a straight IDT, controllable manipulation of 200 fl [302] and 10 fl [303] droplets in a nanofluidic channels have also been achieved. The ability to manipulate droplets in these nanostructures makes it useful for increasing the sensitivity of analytical tools for applications such as medical diagnostics and personalized treatments.

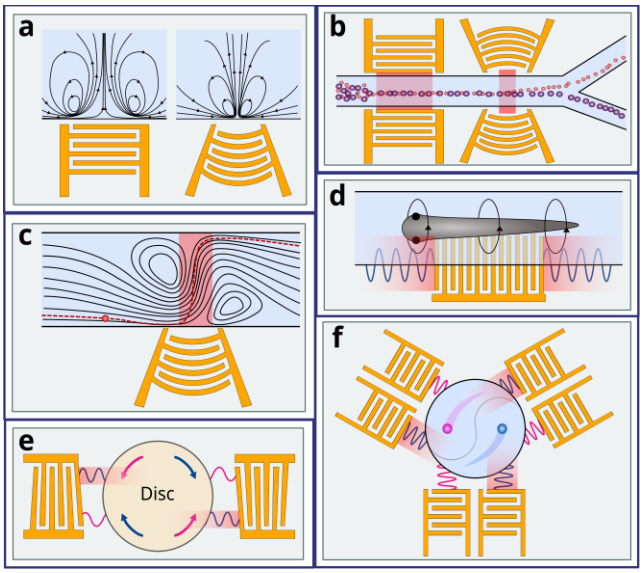

Figure 9. Mixing, concentration, and rotation of liquid in chamber/channel IDT device examples. **(a)** The acoustic streaming generated by straight vs. focused IDT in a closed channel. **(b**) Multistage device for tumor cell isolation. The device consists of pair of straight IDTs for SSAW concentration and a pair of FIDT for TSAW isolation. **(c)** The acoustic streaming of a focused IDT in a continuous flow, acting to direct particle laterally **(d)** Rotational manipulation of zebrafish larvae [36]. The device consists of a straight IDT and a patterned fluidic channel aligned on and parallel to the lateral side of the IDT with half of its width on the IDT. **(e)** A pair of SF-IDT for bidirectional rotating of a thin disc over of fluid coupling layer. **(f)** Tri-directional symmetrical acoustic tweezers for programmable trajectory manipulation [295]. The device comprises six IDTs (divided into two sets) and is symmetrically distributed around an annular-shaped changer at an angle of 120°.

5.2. SSAWs based streaming and acoustofluidics

SSAWs generate…** insert intro SSAW text here like in TSAW section 5.1, and include information on Figure**

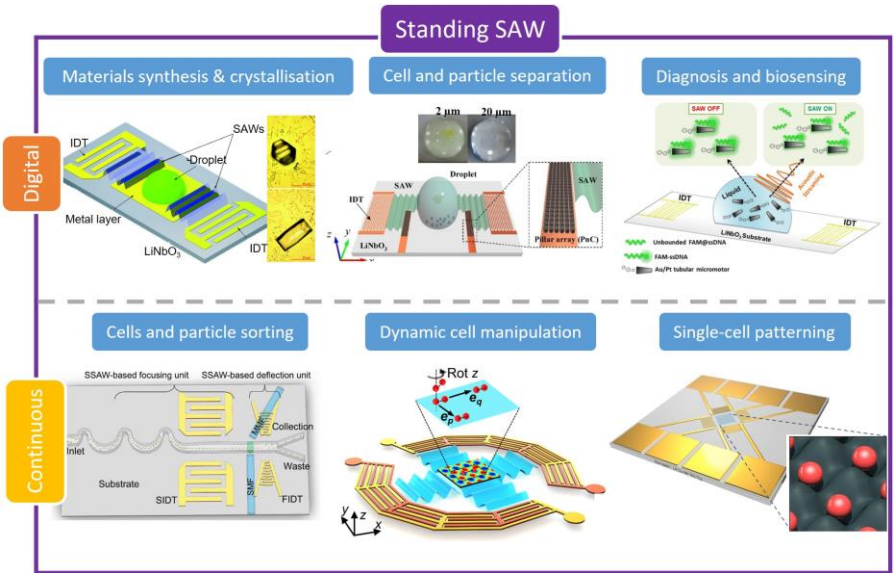

Figure X. Examples of real-life medical applications of SSAW streaming, for both digital and continuous acoustofluidics. **SSAW digital**: **(left)** A SSAW device with drop of glycine solution for crystallization. Reproduced with permission.[304] Copyright 2018, Royal Society of Chemistry. **(middle) A** phononic-crystal device generating scattered SSAW for cell and particle separation. Reproduced with permission.[305] Copyright 2018, Elsevier. **(right)** SSAW device for the removal of molecules that are unbound to micromotors, realized for lowering the detection limit of the cancer-related biomarker miRNA-21. Reproduced with permission.[306] Copyright 2021, American Chemical Society. **SSAW continuous**: **(left)** A SSAW based fluorescence-activated cell sorter with a 3D cell-focusing unit, an in-plane fluorescent detection unit, and a cell-deflection unit on a single chip. Reproduced with permission.[307] Copyright 2018, Wiley. **(middle)** Wave-number acoustic tweezers that enable dynamic reshaping of the SSAW wavefields, achieving dynamic and reconfigurable particle manipulation. Reproduced with permission.[152] Copyright 2019, Science Advances. **(right)** A two-dimensional SSAW device, with four IDTs, for one cell per acoustic well patterning. Reproduced with permission.[308] Copyright 2015, Nature Communications.

5.2.1. SSAW induced droplet streaming in digital acoustofluidics

When SSAWs generated using a pair of IDTs actuate a sessile droplet, it results in symmetric acoustic wave propagations and creates a strong acoustic streaming force inside droplet, even though the droplet might not be easily moved. Therefore, SSAW induced streaming is beneficial for stable mixing and jetting of sessile droplets. For example, SSAW mixing can

increase the kinetic effect to influence the recrystallization process of metal organic frameworks (the best-known being HKUST-1 crystals) [309] and glycine [304] with different morphologies and sizes in a droplet, as well as isolate sodium chloride crystals in a drying droplet [310]. This mixing effect has great potentials in drug delivery and/or release for pharmaceutical industry. The SSAW induced mixing allows for direct, safe and high efficiency mixing, facilitating the dynamic cell culture [311], labelling of nanoparticles [312], or lowering the detection limit for biomarkers [306]. SSAW generated using a pair of small-aperture-straight-electrodes (SASE) in a vertical capillary tube has also been utilized for standardized and controllable droplet jetting [313]. The SASE device has a higher energy density output performance and higher driving capability than large aperture SAW devices which ensures energy concentration and more standardized wave paths [313].

Although droplet transport in liquid within channel is not as easily achieved with SSAWs, it can be achieved by SSAW induced streaming using a pair of straight IDTs in conjunction with anisotropic ratchet conveyors, which use hydrophilic pattens of background to control the directional movement of the droplet transport (Figure 10(a)) [314]. Additionally, this configuration can confine the droplet position to allow for nebulization controlled by the SAW frequency [314]. Scattered SSAWs can be produced using pairs of opposing IDTs and nickel pillar type crystals to control the SAW field (Figure 10(b)). In a sessile droplet, the SSAW can simultaneously induce strong acoustic streaming localized on half a region and directional propagating longitudinal acoustic waves [305]. This mechanism has been used for concentration and separation of 2 and 20 µm PS particles in a microliter droplet [305].

5.2.2. SSAW induced streaming in microchannel for acoustic tweezers in continuous acoustofluidics

The simplest way to generate SSAWs is by using a pair of IDTs. Two counter propagating waves interact, forming a time-averaged nodal and anti-nodal periodic patterning positions across the entire channel [174]. Therefore, SSAWs can easily create one dimensional nodal lines inside channels or chambers [315] for applications such as separation of encapsulated cells [316], extracellular vesicles [284,285] or CTCs [286,287]. For example, tunable cell sorting of human white blood cells (WBC) (15 µm) and fluorescent PS beads (10 µm) was achieved using a pair of chirped IDT and a multi-channel sorting device [317]. This was further developed by acoustically sorting different sizes such as platelets, RBCs and WBC [318]. Tilted angle SSAWs [319] (Figure 10(c)) can be used to increase separation differences between similar sized particles, hence it

can be used for cancer cell manipulation [315] and separating exosomes from whole blood [320]. Phase modulation-based SSAW techniques are another advanced method to increase separation throughput as it uses multiple pressure nodes without the need to increase channel width [321–323].

Multiple IDTs can be easily integrated for such applications, for example, two pairs of IDTs can be used to achieve multi-stage SAW concentration and separation (Figure 10(d)) [324–326]. The first stage is consisted of a pair of IDTs for particle/cell sorting by SSAWs. The second stage is consisted of an IDT, such as a straight IDT, SF-IDT or F-IDT to form TSAWs for particle/cell deflection [288,307,327]. Conventional SSAWs result in particle and cell patterning across the entire width of a microfluidic channel, preventing selective trapping, whereas applying nanosecond-scale pulses can generate localized time-averaged patterning regions for selective trapping [328].

Additional IDTs, for example, two orthogonal pairs of IDTs (Figure 10(e)), [27,329] can be used to form a 2D pattern of nodes and antinodes for particle manipulation [308,330,331]. The 3D spatial distribution of the cells, and preserve the viability and functionality of the patterned cells suitable for tissue engineering applications. In such an orthogonal pair IDT setup, intelligent modulation of harmonic waves can be used to generate time-effective Fourier-synthesized acoustic potential wells, allowing particles/cells in suspended fluids and acoustic lattices to be spatially controlled and reconfigured [332]. Additionally, SSAW generated by SF-IDT can spatially localize cells encapsulated within a gelatibe methacryloyl hydrogel matrix [333]. SSAWs allow particles and cells to be patterned into 3D spatial lines or crystal-lattice-like matrix patterns in chambers of millimeter height [334] (for example, such a chamber is large enough for entire organism manipulation of Caenorhabditis elegans) [141], or formation of multicellular spheroids [335,336]. These SSAW 3D patterns have also been effectively realized using alternative piezoelectric thin film SAW platform such as ZnO or AlN films, instead of $LiNbO_3$ [337].

Acoustic tweezers with generated torque forces using SSAWs could be obtained using a temporal phase lag between the two standing waves, leading to a complex pressure field. The superimposed acoustic streaming induced fluid motion creates stable 3D trapping nodes within a chamber. This method allows for single cell manipulation [338] and controlled rotation and translation of spherical particles or living cells in a 3D format [339]. A wave number-spiral design for acoustic tweezers can enable frequency-based steering of SSAW for simultaneous and independent control. This method only needs two multitone excitation signals which enables

the resultant SAW wavefields to be dynamically reshaped without using complex and costly electronics [152].

SSAWs can also influence the fluid streaming patterns in a chamber. For example, the mixing performance with two opposing parallel straight IDTs (96.7%) is much higher than with one straight IDT (69.8%) as the same applied voltages (85 V_{p-p}) and flow rates (10 µl/min) [340]. The mixing behavior induced by SSAW acoustic streaming can be beneficial in preventing particle deposition in a microchannel [341], or generating microextraction functions for biochemical analysis applications [342,343].

In brief, acoustic tweezers with functions for patterning and particle manipulation based on SSAWs have been a research hot topic in the acoustofluidic field, and have been comprehensively reviewed in many papers [22,24,49,344–346]. Therefore, this paper will not discuss further. For these developments and readers should refer to the above or other review papers for more information.

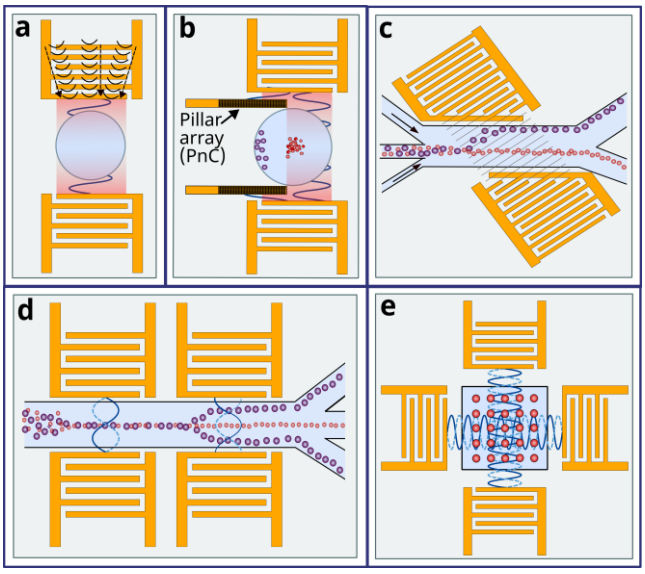

Figure 10. SSAW induced droplet streaming in digital acoustofluidics and microchannel for acoustic tweezers in continuous acoustofluidics IDT device examples. **(a)** A pair of straight IDTs and anisotropic ratchet conveyors for controllable droplet transport [314]. **(b)** A pair of straight IDTs and nickel pillar-type crystal arrays (PnC) which obstruct the lower half of SSAW to produce scattered SSAW for particle concentration and separation [305]. **(c)** Tilted angle SSAW [315] and **(d)** Multi-stage SSAW using two pairs of straight IDTs for particle separation. **(e)** Two orthogonal pairs of IDTs for SSAW particle manipulation (acoustic tweezers).

6. Summary and future prospects

This review aims to elucidate the underlying mechanisms, design methodology, techniques, and applications of acoustic streaming for various acoustofluidic applications. SAW technology is in high demand due to its function as both sensors and actuators in various disciplines. It offers efficient, non-invasive, and biocompatible devices that are valuable for biological research and clinical applications such as diagnosis and therapeutics, health monitoring, and biosampling/treatments. IDTs have their own developed design criteria whereby the IDT materials and geometries, as well as the piezoelectric material, can be changed, allowing for various functions of manipulation control for specific applications. Not only can the device be designed for a specific application, but also it is possible to design programmable features useful for microfluidic processing in applications such as on-chip bioassays, high throughput compound screening and biochemical synthesis. They can also achieve single droplet processing strategies that follow a digital logic rule. The highly sensitive and selective yet simple and low-cost nature of IDTs makes them suitable for lab-on-chip and point-of-care devices.

Acoustic streaming generates regions of recirculation or pressure gradients that lead to rapid and localized motion, allowing it to manipulate particles, such as patterning, concentration, and separation. Such the manipulation is useful for applications such as CTC separation, single cell analysis and even submicron manipulation of exosomes. Acoustic streaming can also generate acoustic pressure or force to perform operations such as deformation, transportation, and manipulation of bulk fluid in a droplet format, namely jetting, nebulization or atomization, microscale streaming, and object rotation. This establishes advanced technologies, such as 3D bioprinting or rotational tweezing for 3D multispectral imaging and digital reconstruction of models.

In brief, this review paper provides qualitative and quantitative descriptions of the acoustic streaming mechanism and recent developments. It presents a snapshot of its remarkable contributions to biomedical research and clinical science. Despite this review showing that much has been accomplished with acoustic streaming-based acoustofluidics, it is important to address that there is a huge amount of work to be done. Some major topics for future development are highlighted as follows.

Mechanisms, theory, and modelling [2,27,50] –

- Analysis techniques need to be further improved. This is because the basic equations used in the analysis have borrowed directly from the classic derivations, which are convenient but might not be accurate for micro or nanoscale acoustofluidics.

- There are specific topics which need to study, for example, nonlinearity, viscous, boundary, inertia, and temperature effects and strongly chaotic phenomena of the waves propagating inside the fluids and its effects on the fluid and particles movements and flow.

- Studies need to be focused on improving computational modelling for acoustic streaming problems in three dimensions for mixed fluids, geometries, and frequency regimes, as well as the nonlinear interactions between the liquid and particles [50].

- The large discrepancy in time and space domains between the driving SAW and the resulting liquid streaming which remains poorly understood. Hence challenges with numerical computational simulations as a very small time step and a very fine mesh are required to capture the SAW actuation of the liquid, but the resulting streaming occurs over a relatively large time scale and large spatial dimensions [27].

- Biological effects of acoustic actuation should be studied at microscopic and nanoscopic length scales and at various time scales.

- Effective nanofabrication and measurement techniques should be utilized to construct nanofluidic devices and study their nanoscale acoustofluidic behaviors.

Device and technique innovations –

- Various substrates and thin film materials, such as those for flexible or wearable ones, polymer-based or hybrid materials with tailored acoustic properties, or new functional platform (e.g., phononic crystals) should be explored for new applications.

- Alternative materials such as electroactive polymer materials technologies apart from a piezoelectric material, or electrets (which have properties much like human muscle tissue) could be explored to design and transform energy between electrical and mechanical forms comparable to piezoelectric materials.

- Disposable superstrates should also be investigated, such as a traditional Petri dish[311,347] or multi-well plates[348], which can make a single SAW-based device reusable and economical by exchanging the superstrates [27].

- Alternate acoustic modes other than SAWs and BAWs could also be explored, which offer unique innovations [27], such as flexural waves[349,350] (Wedge acoustic waves) with acoustic black holes[351].

- Improving heat management methods [50] is important as the heat can affect the sound velocity and hence the resonant frequency. Additionally, heating control is valuable as streaming relies on the acoustic wave being attenuated.

Standardization and commercialization –

- Characterization of the biological effects of the acoustic actuation with the specific frequencies and powers should be standardized so that biomedical researchers can ensure that this technology is suitable for their research or applications [50].

- Open-source codes to compute the acoustic field generated by IDTs should be developed in designing and employing IDT devices for automation and precision control [50].

- All-in-one acoustofluidic prototypes would be advantageous for biomedical research laboratories, which are not need access to external equipment or a high degree of user skills or training, integrated with modern technologies such as mobile phone, touch screen, and Bluetooth, internet [49].

- Costs should be the key consideration for developing the future acoustofluidics devices. The end goal would be their commercialization, ideally with on-chip functionality without requiring extensive and costly external additional equipment such as power supplies, capillary pumps, lasers, and mass spectrometers - all of which at costs acceptable to manufacturers and consumers [48].

Acknowledgments

This work was financially supported by the International Exchange Grants from Royal Society [grant number IEC/NSFC/170142], the UK Engineering and Physical Sciences Research Council (EPSRC) [grant numbers EP/P018998/1 and EP/P002803/1], UK Fluidic Network [EP/N032861/1] Special Interest Group of Acoustofluidics.

7. References

[1] American Scientific (n.d.).
[2] J. Friend and L.Y. Yeo, Rev. Mod. Phys. **83**, 647 (2011).

[3] A. Kundt, Ann. Phys. Chem. **203**, 497 (1866).
[4] V. Dvořák, Annalen Der Physik **233**, 42 (1876).
[5] A. Pavlic and J. Dual, J. Fluid Mech. **911**, A28 (2021).
[6] Lord Rayleigh, Philosophical Transactions of the Royal Society of London **175**, 1 (1884).
[7] Physikalische Zeitschrift. **Vol. 33**, (1932).
[8] P.J. Westervelt, The Journal of the Acoustical Society of America **25**, 60 (1953).
[9] W.L. Nyborg, The Journal of the Acoustical Society of America **25**, 68 (1953).
[10] Y. Gu, C. Chen, J. Rufo, C. Shen, Z. Wang, P.-H. Huang, H. Fu, P. Zhang, S.A. Cummer, Z. Tian, and T.J. Huang, ACS Nano **14**, 14635 (2020).
[11] D.J. Collins, Z. Ma, J. Han, and Y. Ai, Lab Chip **17**, 91 (2016).
[12] G. Destgeer, H. Cho, B.H. Ha, J.H. Jung, J. Park, and H.J. Sung, Lab Chip **16**, 660 (2016).
[13] N. Zhang, J.P. Zuniga-Hertz, E.Y. Zhang, T. Gopesh, M.J. Fannon, J. Wang, Y. Wen, H.H. Patel, and J. Friend, Lab Chip **21**, 904 (2021).
[14] Y. Gu, C. Chen, Z. Mao, H. Bachman, R. Becker, J. Rufo, Z. Wang, P. Zhang, J. Mai, S. Yang, J. Zhang, S. Zhao, Y. Ouyang, D.T.W. Wong, Y. Sadovsky, and T.J. Huang, Sci. Adv. **7**, (2021).
[15] J. Zhou, P. Mukherjee, H. Gao, Q. Luan, and I. Papautsky, APL Bioeng **3**, 041504 (2019).
[16] C. Kumar, M. Hejazian, C. From, S. Saha, E. Sauret, Y. Gu, and N.-T. Nguyen, Physics of Fluids **31**, 063603 (2019).
[17] C. Zhao and C. Yang, Adv Colloid Interface Sci **201–202**, 94 (2013).
[18] A.C. Johnson and M.T. Bowser, Lab Chip **18**, 27 (2017).
[19] B.H. Lapizco-Encinas, ELECTROPHORESIS **40**, 358 (2019).
[20] P. Paiè, T. Zandrini, R.M. Vázquez, R. Osellame, and F. Bragheri, Micromachines (Basel) **9**, E200 (2018).
[21] Y. Wang, Q. Zhang, Z. Zhu, F. Lin, J. Deng, G. Ku, S. Dong, S. Song, M.K. Alam, D. Liu, Z. Wang, and J. Bao, Sci Adv **3**, e1700555 (2017).
[22] A. Ozcelik, J. Rufo, F. Guo, Y. Gu, P. Li, J. Lata, and T.J. Huang, Nat Methods **15**, 1021 (2018).
[23] M.-C.N. Le and Z.H. Fan, Biomed Mater **16**, 022005 (2021).
[24] J. Novotny, A. Lenshof, and T. Laurell, Electrophoresis **43**, 804 (2022).
[25] M.B. Mazalan, A.M. Noor, Y. Wahab, S. Yahud, and W.S.W.K. Zaman, Micromachines (Basel) **13**, 30 (2021).
[26] S. Mohanty, I.S.M. Khalil, and S. Misra, Proc Math Phys Eng Sci **476**, 20200621 (2020).
[27] X. Ding, P. Li, S.-C.S. Lin, Z.S. Stratton, N. Nama, F. Guo, D. Slotcavage, X. Mao, J. Shi, F. Costanzo, and T.J. Huang, Lab Chip **13**, 3626 (2013).
[28] D. Mandal and S. Banerjee, Sensors (Basel) **22**, 820 (2022).
[29] M.K. Tan, J.R. Friend, and L.Y. Yeo, Phys. Rev. Lett. **103**, 024501 (2009).
[30] M. Jangi, J.T. Luo, R. Tao, J. Reboud, R. Wilson, J.M. Cooper, D. Gibson, and Y.Q. Fu, International Journal of Multiphase Flow **114**, 1 (2019).
[31] D.J. Collins, O. Manor, A. Winkler, H. Schmidt, J.R. Friend, and L.Y. Yeo, Phys Rev E Stat Nonlin Soft Matter Phys **86**, 056312 (2012).
[32] C. Cortez-Jugo, A. Qi, A. Rajapaksa, J.R. Friend, and L.Y. Yeo, Biomicrofluidics **9**, (2015).
[33] J. Wang, H. Hu, A. Ye, J. Chen, and P. Zhang, Sensors and Actuators A: Physical **238**, 1 (2016).
[34] J. Zhou, X. Tao, J. Luo, Y. Li, H. Jin, S. Dong, J. Luo, H. Duan, and Y. Fu, Surface and Coatings Technology **367**, 127 (2019).
[35] E. Galopin, M. Beaugeois, B. Pinchemel, J.-C. Camart, M. Bouazaoui, and V. Thomy, Biosensors and Bioelectronics **23**, 746 (2007).
[36] C. Chen, Y. Gu, J. Philippe, P. Zhang, H. Bachman, J. Zhang, J. Mai, J. Rufo, J.F. Rawls, E.E. Davis, N. Katsanis, and T.J. Huang, Nat Commun **12**, 1118 (2021).
[37] J. Zhang, S. Yang, C. Chen, J.H. Hartman, P.-H. Huang, L. Wang, Z. Tian, P. Zhang, D. Faulkenberry, J.N. Meyer, and T.J. Huang, Lab Chip **19**, 984 (2019).
[38] S. Marqus, L. Lee, T. Istivan, R.Y. Kyung Chang, C. Dekiwadia, H.-K. Chan, and L.Y. Yeo, European Journal of Pharmaceutics and Biopharmaceutics **151**, 181 (2020).

[39] Z. Gong, L. Huang, X. Tang, K. Chen, Z. Wu, L. Zhang, Y. Sun, Y. Xia, H. Chen, Y. Wei, F. Wang, and S. Guo, Advanced Healthcare Materials **10**, 2101312 (2021).
[40] Y. Wang, Q. Zhang, R. Tao, J. Xie, P. Canyelles-Pericas, H. Torun, J. Reboud, G. McHale, L.E. Dodd, X. Yang, J. Luo, Q. Wu, and Y. Fu, ACS Appl Mater Interfaces **13**, 16978 (2021).
[41] H. Lim, S.M. Back, H. Choi, and J. Nam, Lab Chip **20**, 120 (2019).
[42] T. Inui, J. Mei, C. Imashiro, Y. Kurashina, J. Friend, and K. Takemura, Lab Chip (2021).
[43] J.H. Jung, G. Destgeer, J. Park, H. Ahmed, K. Park, and H.J. Sung, RSC Adv. **8**, 3206 (2018).
[44] J. Nam, W.S. Jang, J. Kim, H. Lee, and C.S. Lim, Biosensors and Bioelectronics **142**, 111496 (2019).
[45] P. Zhang, Sci Adv **6**, 0606, (2020).
[46] S. Zhang, Y. Wang, P. Onck, and J. den Toonder, Microfluid Nanofluid **24**, 24 (2020).
[47] W. Connacher, N. Zhang, A. Huang, J. Mei, S. Zhang, T. Gopesh, and J. Friend, Lab on a Chip **18**, 1952 (2018).
[48] L.Y. Yeo, H.-C. Chang, P.P.Y. Chan, and J.R. Friend, Small **7**, 12 (2011).
[49] P. Zhang, H. Bachman, A. Ozcelik, and T.J. Huang, Annu Rev Anal Chem (Palo Alto Calif) **13**, 17 (2020).
[50] J. Rufo, F. Cai, J. Friend, M. Wiklund, and T.J. Huang, Nat Rev Methods Primers **2**, 1 (2022).
[51] J. Rufo, P. Zhang, R. Zhong, L.P. Lee, and T.J. Huang, Nat Commun **13**, 3459 (2022).
[52] C.K. Campbell, Proc. IEEE **77**, 1453 (1989).
[53] A.V. Mamishev, K. Sundara-Rajan, F. Yang, Y. Du, and M. Zahn, Proceedings of the IEEE **92**, 808 (2004).
[54] S. Datta, *Surface Acoustic Wave Devices* (Prentice-Hall, 1986).
[55] C.K. Campbell, *Surface Acoustic Wave Devices for Mobile and Communication Applications* (Academic Press, 1998).
[56] V. Plessky and L. Reindl, IEEE Trans. Ultrason. Ferroelectr. Fre. Control **57**, 654 (2010).
[57] Y.Q. Fu, J.K. Luo, N.T. Nguyen, A.J. Walton, A.J. Flewitt, X.T. Zu, Y. Li, G. McHale, A. Matthews, E. Iborra, H. Du, and W.I. Milne, Progress in Materials Science **89**, 31 (2017).
[58] M. Wu, K. Chen, S. Yang, Z. Wang, P.-H. Huang, J. Mai, Z.-Y. Li, and T.J. Huang, Lab Chip **18**, 3003 (2018).
[59] M. Wu, P.-H. Huang, R. Zhang, Z. Mao, C. Chen, G. Kemeny, P. Li, A.V. Lee, R. Gyanchandani, A.J. Armstrong, M. Dao, S. Suresh, and T.J. Huang, Small **14**, 1801131 (2018).
[60] J. Nam, H. Lim, and S. Shin, Korea-Aust. Rheol. J. **23**, 255 (2011).
[61] G. Zhang, *Bulk and Surface Acoustic Waves: Fundamentals, Devices, and Applications* (Jenny Stanford Publishing, New York, 2022).
[62] Y.-Q. Fu, H.-F. Pang, H. Torun, R. Tao, G. McHale, J. Reboud, K. Tao, J. Zhou, J. Luo, D. Gibson, J. Luo, and P. Hu, Lab Chip **21**, 254 (2021).
[63] S. Song, Q. Wang, J. Zhou, and A. Riaud, Nanotechnology and Precision Engineering **5**, 035001 (2022).
[64] M.P. Nair, A.J.T. Teo, and K.H.H. Li, Micromachines (Basel) **13**, 24 (2021).
[65] R. Fogel, J. Limson, and A.A. Seshia, Essays Biochem **60**, 101 (2016).
[66] K. Länge, Sensors (Basel) **19**, E5382 (2019).
[67] A. Mujahid and F.L. Dickert, Sensors (Basel) **17**, E2716 (2017).
[68] G. Destgeer, B.H. Ha, J.H. Jung, and H.J. Sung, Lab Chip **14**, 4665 (2014).
[69] D. Malocha, (2000).
[70] D.P. Morgans, *Surface Acoustic Wave Devices for Signal Processing* (Elsevier, 1991).
[71] M. Feldmann and J. Henaff, (1989).
[72] J.S. Bach and H. Bruus, Phys. Rev. Lett. **124**, 214501 (2020).
[73] H. Bruus, Lab Chip **12**, 20 (2012).
[74] J. Lei, P. Glynne-Jones, and M. Hill, Microfluid Nanofluid **21**, 23 (2017).
[75] S.S. Sadhal, Lab Chip **12**, 2292 (2012).
[76] S. Boluriaan and P.J. Morris, International Journal of Aeroacoustics **2**, 255 (2003).

[77] B.E. Rapp, in *Microfluidics: Modelling, Mechanics and Mathematics*, edited by B.E. Rapp (Elsevier, Oxford, 2017), pp. 243–263.
[78] L.K. Zarembo, in *High-Intensity Ultrasonic Fields*, edited by L.D. Rozenberg (Springer US, Boston, MA, 1971), pp. 135–199.
[79] M. Evander and J. Nilsson, Lab Chip **12**, 4667 (2012).
[80] M. Settnes and H. Bruus, Phys. Rev. E **85**, 016327 (2012).
[81] H. Bruus, Lab Chip **12**, 1014 (2012).
[82] S. Liu, Y. Yang, Z. Ni, X. Guo, L. Luo, J. Tu, D. Zhang, and J. Zhang, Sensors (Basel) **17**, 1664 (2017).
[83] R. Barnkob, P. Augustsson, T. Laurell, and H. Bruus, Phys Rev E Stat Nonlin Soft Matter Phys **86**, 056307 (2012).
[84] P. Glynne-Jones and M. Hill, Lab Chip **13**, 1003 (2013).
[85] J. Shi, H. Huang, Z. Stratton, Y. Huang, and T.J. Huang, Lab Chip **9**, 3354 (2009).
[86] M. Wiklund, R. Green, and M. Ohlin, Lab Chip **12**, 2438 (2012).
[87] S.J. Lighthill, Journal of Sound and Vibration **61**, 391 (1978).
[88] T. Laurell and A. Lenshof, *Microscale Acoustofluidics* (Royal Society of Chemistry, 2014).
[89] X. Luo, J. Cao, H. Gong, H. Yan, and L. He, Ultrasonics Sonochemistry **48**, 287 (2018).
[90] C. Devendran, T. Albrecht, J. Brenker, T. Alan, and A. Neild, Lab Chip **16**, 3756 (2016).
[91] K. Sritharan, C.J. Strobl, M.F. Schneider, A. Wixforth, and Z. Guttenberg, Appl. Phys. Lett. **88**, 054102 (2006).
[92] J.K. Luo, Y.Q. Fu, and W.I. Milne, Modeling and Measurement Methods for Acoustic Waves and for Acoustic Microdevices (2013).
[93] J. Li, M.H. Biroun, R. Tao, Y. Wang, H. Torun, N. Xu, M. Rahmati, Y. Li, D. Gibson, C. Fu, J. Luo, L. Dong, J. Xie, and Y. Fu, J. Phys. D: Appl. Phys. **53**, 355402 (2020).
[94] Z. Guttenberg, A. Rathgeber, S. Keller, J.O. Rädler, A. Wixforth, M. Kostur, M. Schindler, and P. Talkner, Phys. Rev. E **70**, 056311 (2004).
[95] R.M. Arzt, E. Salzmann, and K. Dransfeld, Applied Physics Letters **10**, 165 (1967).
[96] M.K. Tan, L.Y. Yeo, and J.R. Friend, EPL **87**, 47003 (2009).
[97] N. Riley, Annual Review of Fluid Mechanics **33**, 43 (2001).
[98] N. Nama, R. Barnkob, Z. Mao, C.J. Kähler, F. Costanzo, and T.J. Huang, Lab Chip **15**, 2700 (2015).
[99] A. Riaud, M. Baudoin, O. Bou Matar, J.-L. Thomas, and P. Brunet, J. Fluid Mech. **821**, 384 (2017).
[100] S. Sachs, M. Baloochi, C. Cierpka, and J. König, Lab Chip **22**, 2011 (2022).
[101] T. Bui, V. Nguyen, S. Vollebregt, B. Morana, H. van Zeijl, T. Chu Duc, and P.M. Sarro, Applied Surface Science **426**, 253 (2017).
[102] M. Wu, A. Ozcelik, J. Rufo, Z. Wang, R. Fang, and T. Jun Huang, Microsyst Nanoeng **5**, (2019).
[103] G. Destgeer, J.H. Jung, J. Park, H. Ahmed, and H.J. Sung, Anal. Chem. **89**, 736 (2017).
[104] D.-T. Phan and G.-S. Chung, Applied Surface Science **257**, 8696 (2011).
[105] A. Winkler, R. Brünig, C. Faust, R. Weser, and H. Schmidt, Sensors and Actuators A: Physical **247**, 259 (2016).
[106] M.-I. Rocha-Gaso, Y. Jimenez, L.A. Francis, and A. Arnau, in (2013).
[107] J. Kirschner, in (2010).
[108] Aw. R.Weser and Sm. M.Weihnacht, Ultrasonics **106**, 106160 (2020).
[109] E. Ntagwirumugara, T. Gryba, V.Y. Zhang, E. Dogheche, and J.-E. Lefebvre, IEEE Transactions on Ultrasonics, Ferroelectrics, and Frequency Control **54**, 2011 (2007).
[110] M. Akiyama, K. Nagao, N. Ueno, H. Tateyama, and T. Yamada, Vacuum **74**, 699 (2004).
[111] A. Vorobiev and S. Gevorgian, IEEE Transactions on Ultrasonics, Ferroelectrics, and Frequency Control **61**, 840 (2014).
[112] W. Soluch and E. Brzozowski, IEEE Transactions on Electron Devices **61**, 3395 (2014).
[113] J. Chen, X. He, W. Wang, W. Xuan, J. Zhou, X. Wang, S.R. Dong, S. Garner, P. Cimo, and J.K. Luo, Journal of Materials Chemistry C **2**, 9109 (2014).
[114] J. Zhou, X.Z. Wu, D.B. Xiao, M. Zhuo, H. Jin, J.K. Luo, and Y.Q. Fu, Surface and Coatings Technology **320**, 39 (2017).

[115] V. Mišeikis, R.J. Shilton, M. Travagliati, M. Agostini, M. Cecchini, V. Piazza, and C. Coletti, Nanotechnology **32**, 375503 (2021).
[116] J. Zhou, J. Zheng, X. Shi, Z. Chen, J. Wu, S. Xiong, J. Luo, S. Dong, H. Jin, H. Duan, and Y. Fu, J. Electrochem. Soc. **166**, B432 (2019).
[117] Y. Yao and Y. Xue, Sensors and Actuators B: Chemical **222**, 755 (2016).
[118] A.S. Mayorov, N. Hunter, W. Muchenje, C.D. Wood, M. Rosamond, E.H. Linfield, A.G. Davies, and J.E. Cunningham, Applied Physics Letters **104**, 083509 (2014).
[119] D. Roshchupkin, L. Ortega, I. Zizak, O. Plotitcyna, V. Matveev, O. Kononenko, E. Emelin, A. Erko, K. Tynyshtykbayev, and D. Irzhak, Journal of Applied Physics **118**, 104901 (2015).
[120] J. Zhou, X. Shi, D. Xiao, X. Wu, J. Zheng, J. Luo, M. Zhuo, X. Tao, H. Jin, S. Dong, R. Tao, H. Duan, and Y. Fu, J. Micromech. Microeng. **29**, 015006 (2019).
[121] M. Darmawan and D. Byun, Microfluidics and Nanofluidics **18**, 1107 (2015).
[122] Y.Q. Fu, L. Garcia-Gancedo, H.F. Pang, S. Porro, Y.W. Gu, J.K. Luo, X.T. Zu, F. Placido, J.I.B. Wilson, A.J. Flewitt, and W.I. Milne, Biomicrofluidics **6**, 24105 (2012).
[123] H. Jin, J. Zhou, X. He, W. Wang, H. Guo, S. Dong, D. Wang, Y. Xu, J. Geng, J.K. Luo, and W.I. Milne, Sci Rep **3**, 2140 (2013).
[124] D.-S. Lee, J. Luo, Y. Fu, W.I. Milne, N.-M. Park, S.H. Kim, M.Y. Jung, and S. Maeng, J Nanosci Nanotechnol **8**, 4626 (2008).
[125] C. Sun, F. Wu, Y. Fu, D.J. Wallis, R. Mikhaylov, F. Yuan, D. Liang, Z. Xie, H. Wang, R. Tao, M.H. Shen, J. Yang, W. Xun, Z. Wu, Z. Yang, H. Cang, and X. Yang, Ultrasonics **108**, 106202 (2020).
[126] C. Sun, F. Wu, D.J. Wallis, M.H. Shen, F. Yuan, J. Yang, J. Wu, Z. Xie, D. Liang, H. Wang, R. Tickle, R. Mikhaylov, A. Clayton, Y. Zhou, Z. Wu, Y. Fu, W. Xun, and X. Yang, IEEE Transactions on Electron Devices **67**, 3355 (2020).
[127] S. Büyükköse, B. Vratzov, J. van der Veen, P.V. Santos, and W.G. van der Wiel, Appl. Phys. Lett. **102**, 013112 (2013).
[128] S. Büyükköse, B. Vratzov, D. Ataç, J. van der Veen, P.V. Santos, and W.G. van der Wiel, Nanotechnology **23**, 315303 (2012).
[129] J. Zhou, D. Zhang, Y. Liu, F. Zhuo, L. Qian, H. Li, Y.-Q. Fu, and H. Duan, Engineering S2095809922003575 (2022).
[130] R. Mikhaylov, F. Wu, H. Wang, A. Clayton, C. Sun, Z. Xie, D. Liang, Y. Dong, F. Yuan, D. Moschou, Z. Wu, M.H. Shen, J. Yang, Y. Fu, Z. Yang, C. Burton, R.J. Errington, M. Wiltshire, and X. Yang, Lab Chip **20**, 1807 (2020).
[131] R. Mikhaylov, M.S. Martin, P. Dumcius, H. Wang, F. Wu, X. Zhang, V. Akhimien, C. Sun, A. Clayton, Y. Fu, L. Ye, Z. Dong, Z. Wu, and X. Yang, J. Micromech. Microeng. **31**, 074003 (2021).
[132] S. Zahertar, H. Torun, C. Sun, C. Markwell, Y. Dong, X. Yang, and Y. Fu, Sensors **22**, 4344 (2022).
[133] Z. Ma, A.J.T. Teo, S.H. Tan, Y. Ai, and N.-T. Nguyen, Micromachines (Basel) **7**, (2016).
[134] A.R. Rezk, J.R. Friend, and L.Y. Yeo, Lab Chip **14**, 1802 (2014).
[135] R.P. Hodgson, M. Tan, L. Yeo, and J. Friend, Appl. Phys. Lett. **94**, 024102 (2009).
[136] C. Fu, K. Lee, K. Lee, S.S. Yang, and W. Wang, Sensors and Actuators A: Physical **218**, 80 (2014).
[137] S. Lehtonen, V.P. Plessky, C.S. Hartmann, and M.M. Salomaa, IEEE Transactions on Ultrasonics, Ferroelectrics, and Frequency Control **51**, 1697 (2004).
[138] H. Nakamura, T. Yamada, T. Ishizaki, and K. Nishimura, IEEE Transactions on Microwave Theory and Techniques **49**, 761 (2001).
[139] M.M. de Lima Jr, F. Alsina, W. Seidel, and P.V. Santos, Journal of Applied Physics **94**, 7848 (2003).
[140] T.-T. Wu, H.-T. Tang, Y.-Y. Chen, and P.-L. Liu, IEEE Transactions on Ultrasonics, Ferroelectrics, and Frequency Control **52**, 1384 (2005).
[141] X. Ding, S.-C.S. Lin, B. Kiraly, H. Yue, S. Li, I.-K. Chiang, J. Shi, S.J. Benkovic, and T.J. Huang, Proceedings of the National Academy of Sciences **109**, 11105 (2012).
[142] M. Lamothe, V. Plessky, J.-M. Friedt, T. Ostertag, and S. Ballandras, Electronics Letters **49**, 1576 (2013).
[143] V. Plessky and M. Lamothe, Electronics Letters **49**, 1503 (2013).

[144] T. Frommelt, M. Kostur, M. Wenzel-Schäfer, P. Talkner, P. Hänggi, and A. Wixforth, Physical Review Letters **100**, 034502 (2008).
[145] X. Ding, J. Shi, S.-C. Steven Lin, S. Yazdi, B. Kiraly, and T. Jun Huang, Lab on a Chip **12**, 2491 (2012).
[146] Y. Chen, X. Ding, S.-C. Steven Lin, S. Yang, P.-H. Huang, N. Nama, Y. Zhao, A.A. Nawaz, F. Guo, W. Wang, Y. Gu, T.E. Mallouk, and T.J. Huang, ACS Nano **7**, 3306 (2013).
[147] H. Mansoorzare and R. Abdolvand, in *2022 IEEE 35th International Conference on Micro Electro Mechanical Systems Conference (MEMS)* (2022), pp. 1014–1017.
[148] V. Laude, D. Gérard, N. Khelfaoui, C. Jerez-Hanckes, S. Benchabane, H. Moubchir, and A. Khelif, in (2007), pp. 2115–2118.
[149] S. Zaehringer and N. Schwesinger, Microsystem Technologies **16**, 871 (2010).
[150] R. O'Rorke, A. Winkler, D. Collins, and Y. Ai, RSC Adv. **10**, 11582 (2020).
[151] C. Pan, G. Xiao, Z. Feng, and W.-H. Liao, Smart Mater. Struct. **23**, 125029 (2014).
[152] Z. Tian, S. Yang, P.-H. Huang, Z. Wang, P. Zhang, Y. Gu, H. Bachman, C. Chen, M. Wu, Y. Xie, and T.J. Huang, Sci. Adv. **5**, eaau6062 (2019).
[153] G.J. Xiao, C.L. Pan, Y.B. Liu, and Z.H. Feng, Sensors and Actuators A: Physical **227**, 1 (2015).
[154] C.L. Pan, Y.T. Ma, Y.B. Liu, Q. Zhang, and Z.H. Feng, Sensors and Actuators A: Physical **148**, 250 (2008).
[155] S.V. Biryukov, G. Martin, and M. Weihnacht, Appl. Phys. Lett. **90**, 173503 (2007).
[156] P. Kang, Z. Tian, S. Yang, W. Yu, H. Zhu, H. Bachman, S. Zhao, P. Zhang, Z. Wang, R. Zhong, and T.J. Huang, Lab Chip **20**, 987 (2020).
[157] A. Riaud, M. Baudoin, J.-L. Thomas, and O. Bou Matar, IEEE Transactions on Ultrasonics, Ferroelectrics, and Frequency Control **63**, 1601 (2016).
[158] A. Riaud, J.-L. Thomas, E. Charron, A. Bussonnière, O. Bou Matar, and M. Baudoin, Physical Review Applied **4**, 034004 (2015).
[159] Z. Tian, Sci Adv **6**, 0494, (2020).
[160] M. Baudoin, J.-C. Gerbedoen, A. Riaud, O.B. Matar, N. Smagin, and J.-L. Thomas, Science Advances **5**, eaav1967 (2019).
[161] T. Tsuji, R. Mihara, T. Saito, S. Hagihara, T. Oizumi, N. Takeda, T. Ohgi, T. Yanagisawa, S. Akao, N. Nakaso, and K. Yamanaka, Materials Transactions **55**, 1040 (2014).
[162] M. Mańka, M. Rosiek, A. Martowicz, T. Stepinski, and T. Uhl, Mechanical Systems and Signal Processing **78**, 71 (2016).
[163] J. Zhu, N.W. Emanetoglu, Y. Lu, J.A. Kosinski, and R.A. Pastore, IEEE Transactions on Ultrasonics, Ferroelectrics, and Frequency Control **48**, 1383 (2001).
[164] M.M. de Lima and P.V. Santos, Rep. Prog. Phys. **68**, 1639 (2005).
[165] M.M. de Lima Jr, W. Seidel, H. Kostial, and P.V. Santos, Journal of Applied Physics **96**, 3494 (2004).
[166] Q. Zhang, T. Han, G. Tang, J. Chen, and K. Hashimoto, in *2015 IEEE International Ultrasonics Symposium (IUS)* (2015), pp. 1–4.
[167] Q. Zhang, T. Han, J. Chen, W. Wang, and K. Hashimoto, Diamond and Related Materials **58**, 31 (2015).
[168] S.F. Hon, K.W. Kwok, H.L. Li, and H.Y. Ng, Review of Scientific Instruments **81**, 065102 (2010).
[169] K.W. Kwok, S.F. Hon, and D. Lin, Sensors and Actuators A: Physical **168**, 168 (2011).
[170] C.-Y. Lee, W. Pang, H. Yu, and E.S. Kim, Appl. Phys. Lett. **93**, 034104 (2008).
[171] K. Kalantar-Zadeh, D.A. Powell, W. Wlodarski, S. Ippolito, and K. Galatsis, Sensors and Actuators B: Chemical **91**, 303 (2003).
[172] W.-C. Shih, H.-Y. Su, and M.-S. Wu, Thin Solid Films **517**, 3378 (2009).
[173] O. Legrani, O. Elmazria, S. Zhgoon, P. Pigeat, and A. Bartasyte, IEEE Sensors Journal **13**, 487 (2013).
[174] A. Fakhfouri, C. Devendran, A. Ahmed, J. Soria, and A. Neild, Lab Chip **18**, 3926 (2018).
[175] R.J. Shilton, M. Travagliati, F. Beltram, and M. Cecchini, Advanced Materials **26**, 4941 (2014).
[176] S.P. Zhang, J. Lata, C. Chen, J. Mai, F. Guo, Z. Tian, L. Ren, Z. Mao, P.-H. Huang, P. Li, S. Yang, and T.J. Huang, Nature Communications **9**, 2928 (2018).

[177] Z. Ma, D.J. Collins, and Y. Ai, Anal. Chem. **88**, 5316 (2016).
[178] C. Sun, Y. Dong, J. Wei, M. Cai, D. Liang, Y. Fu, Y. Zhou, Y. Sui, F. Wu, R. Mikhaylov, H. Wang, F. Fan, Z. Xie, M. Stringer, Z. Yang, Z. Wu, L. Tian, and X. Yang, Acta Biomaterialia (2022).
[179] A.L. Zhang, Z.Q. Wu, and X.H. Xia, Talanta **84**, 293 (2011).
[180] L.G. Schnitzler, S. Junger, D.M. Loy, E. Wagner, A. Wixforth, A. Hörner, U. Lächelt, and C. Westerhausen, J. Phys. D: Appl. Phys. **52**, 244002 (2019).
[181] M.K. Tan, J.R. Friend, and L.Y. Yeo, Lab Chip **7**, 618 (2007).
[182] S.K.R.S. Sankaranarayanan, S. Cular, V.R. Bhethanabotla, and B. Joseph, Phys. Rev. E **77**, 066308 (2008).
[183] J. Liu, S. Li, and V.R. Bhethanabotla, ACS Sens. **3**, 222 (2018).
[184] Y. Li, Y.Q. Fu, S.D. Brodie, M. Alghane, and A.J. Walton, Biomicrofluidics **6**, 12812 (2012).
[185] A.N. Darinskii, M. Weihnacht, and H. Schmidt, Journal of Applied Physics **123**, 014902 (2018).
[186] M. Djukelic, A. Wixforth, and C. Westerhausen, Biomicrofluidics **11**, 024115 (2017).
[187] D. Peng, W. Tong, D.J. Collins, M.R. Ibbotson, S. Prawer, and M. Stamp, Frontiers in Neuroscience **15**, 37 (2021).
[188] E.M. Kugler, K. Michel, D. Kirchenbüchler, G. Dreissen, A. Csiszár, R. Merkel, M. Schemann, and G. Mazzuoli-Weber, Neuroscience **372**, 213 (2018).
[189] R. Ravin, P.S. Blank, A. Steinkamp, S.M. Rappaport, N. Ravin, L. Bezrukov, H. Guerrero-Cazares, A. Quinones-Hinojosa, S.M. Bezrukov, and J. Zimmerberg, PLoS One **7**, e39421 (2012).
[190] N. Sivanantha, C. Ma, D.J. Collins, M. Sesen, J. Brenker, R.L. Coppel, A. Neild, and T. Alan, Appl. Phys. Lett. **105**, 103704 (2014).
[191] A.M. Jötten, S. Angermann, M.E.M. Stamp, D. Breyer, F.G. Strobl, A. Wixforth, and C. Westerhausen, RSC Adv. **9**, 543 (2018).
[192] U. Farooq, X. Liu, W. Zhou, M. Hassan, L. Niu, and L. Meng, Sensors and Actuators B: Chemical **345**, 130335 (2021).
[193] A. Bussonnière, Y. Miron, M. Baudoin, O. Bou Matar, M. Grandbois, P. Charette, and A. Renaudin, Lab Chip **14**, 3556 (2014).
[194] P. Gelin, Ö. Sardan Sukas, K. Hellemans, D. Maes, and W. De Malsche, Chemical Engineering Journal **369**, 370 (2019).
[195] P.R. Rogers, J.R. Friend, and L.Y. Yeo, Lab Chip **10**, 2979 (2010).
[196] H. Li, J.R. Friend, and L.Y. Yeo, Biomed Microdevices **9**, 647 (2007).
[197] R. Singh, S.K.R.S. Sankaranarayanan, and V.R. Bhethanabotla, Journal of Applied Physics **107**, 024503 (2010).
[198] J. Friend, L. Yeo, M. Tan, and R. Shilton, in *Proceedings - IEEE Ultrasonics Symposium* (IEEE, 2008), pp. 930–933.
[199] R. Shilton, M.K. Tan, L.Y. Yeo, and J.R. Friend, Journal of Applied Physics **104**, (2008).
[200] Y. Bourquin, A. Syed, J. Reboud, L.C. Ranford-Cartwright, M.P. Barrett, and J.M. Cooper, Angew Chem Int Ed Engl **53**, 5587 (2014).
[201] Z. Wang, J. Rich, N. Hao, Y. Gu, C. Chen, S. Yang, P. Zhang, and T.J. Huang, Microsyst Nanoeng **8**, 1 (2022).
[202] W. Liang, F. Zhang, G. Yang, and Z. Wang, Microfluidics and Nanofluidics **21**, 2 (2017).
[203] J.H. Jung, G. Destgeer, B. Ha, J. Park, and H.J. Sung, Lab Chip **16**, 3235 (2016).
[204] S. Collignon, J. Friend, and L. Yeo, Lab on a Chip **15**, 1942 (2015).
[205] Z. Guttenberg, H. Müller, H. Habermüller, A. Geisbauer, J. Pipper, J. Felbel, M. Kielpinski, J. Scriba, and A. Wixforth, Lab on a Chip **5**, 308 (2005).
[206] J.-Y. Bao and A.-L. Zhang, Ferroelectrics **558**, 199 (2020).
[207] A. Zhang, Y. Zha, and J. Zhang, AIP Advances **4**, 127144 (2014).
[208] P. Brunet, M. Baudoin, O.B. Matar, and F. Zoueshtiagh, Physical Review E - Statistical, Nonlinear, and Soft Matter Physics **81**, (2010).
[209] D. Beyssen, L. Le Brizoual, O. Elmazria, and P. Alnot, Sensors and Actuators, B: Chemical **118**, 380 (2006).

[210] M. Baudoin, P. Brunet, O.B. Matar, and E. Herth, Applied Physics Letters **100**, 154102 (2012).
[211] X.Y. Du, M.E. Swanwick, Y.Q. Fu, J.K. Luo, A.J. Flewitt, D.S. Lee, S. Maeng, and W.I. Milne, Journal of Micromechanics and Microengineering **19**, 035016 (2009).
[212] J.T. Luo, N.R. Geraldi, J.H. Guan, G. McHale, G.G. Wells, and Y.Q. Fu, Physical Review Applied **7**, 014017 (2017).
[213] L. Wu, Z. Guo, and W. Liu, Advances in Colloid and Interface Science **308**, 102770 (2022).
[214] Y. Wang, X. Tao, R. Tao, J. Zhou, Q. Zhang, D. Chen, H. Jin, S. Dong, J. Xie, and Y.Q. Fu, Sensors and Actuators A: Physical **306**, 111967 (2020).
[215] R. Tao, G. Mchale, J. Reboud, J.M. Cooper, H. Torun, J.T. Luo, J. Luo, X. Yang, J. Zhou, P. Canyelles-Pericas, Q. Wu, and Y. Fu, Nano Letters **20**, 3263 (2020).
[216] A.-L. Zhang and X.-H. Xia, Chinese Journal of Analytical Chemistry **39**, 765 (2011).
[217] Y. Ai and B.L. Marrone, Microfluid Nanofluid **13**, 715 (2012).
[218] A. Wixforth, C. Strobl, Ch. Gauer, A. Toegl, J. Scriba, and Z. v. Guttenberg, Anal Bioanal Chem **379**, 982 (2004).
[219] C. Chen, S.P. Zhang, Z. Mao, N. Nama, Y. Gu, P.-H. Huang, Y. Jing, X. Guo, F. Costanzo, and T.J. Huang, Lab Chip **18**, 3645 (2018).
[220] D.S. Brodie, Y.Q. Fu, Y. Li, M. Alghane, R.L. Reuben, and A.J. Walton, Appl. Phys. Lett. **99**, 153704 (2011).
[221] C. Fu, A.J. Quan, J.T. Luo, H.F. Pang, Y.J. Guo, Q. Wu, W.P. Ng, X.T. Zu, and Y.Q. Fu, Appl. Phys. Lett. **110**, 173501 (2017).
[222] P.K. Bhattacharjee, A.G. McDonnell, R. Prabhakar, L.Y. Yeo, and J. Friend, New Journal of Physics **13**, (2011).
[223] J.O. Castro, S. Ramesan, A.R. Rezk, and L.Y. Yeo, Soft Matter **14**, 5721 (2018).
[224] R. Li, Z. Gong, Z. Wu, H. Chen, Y. Xia, Y. Liu, F. Wang, and S. Guo, Nano Futures **4**, 045001 (2020).
[225] R. Li, Z. Gong, K. Yi, W. Li, Y. Liu, F. Wang, and S. Guo, ACS Appl. Bio Mater. **3**, 6521 (2020).
[226] X. Wei, K. Chen, B. Cai, L. Rao, Z. Wang, Y. Sun, M. Yu, W. Liu, S. Guo, and X.-Z. Zhao, ACS Appl. Mater. Interfaces **11**, 41118 (2019).
[227] Y. Xia, L.-X. Huang, H. Chen, J. Li, K.-K. Chen, H. Hu, F.-B. Wang, Z. Ding, and S.-S. Guo, ACS Appl. Mater. Interfaces **13**, 12950 (2021).
[228] K. Chen, E. Jiang, X. Wei, Y. Xia, Z. Wu, Z. Gong, Z. Shang, and S. Guo, Lab on a Chip **21**, 1604 (2021).
[229] D. Lee, N. Lee, G. Choi, and H.H. Cho, Inventions **3**, 38 (2018).
[230] A.R. Rezk, J.K. Tan, and L.Y. Yeo, Advanced Materials **28**, 1970 (2016).
[231] A.R. Rezk, S. Ramesan, and L.Y. Yeo, Lab Chip **18**, 406 (2018).
[232] U. Demirci, Journal of Microelectromechanical Systems **15**, 957 (2006).
[233] K. Chen, C. Sui, Y. Wu, Z. Ao, S.S. Guo, and F. Guo, Nanotechnology **30**, 084001 (2018).
[234] V. Laude, D. Gérard, N. Khelfaoui, C.F. Jerez-Hanckes, S. Benchabane, and A. Khelif, Appl. Phys. Lett. **92**, 094104 (2008).
[235] J. Zhou, H.F. Pang, L. Garcia-Gancedo, E. Iborra, M. Clement, M. De Miguel-Ramos, H. Jin, J.K. Luo, S. Smith, S.R. Dong, D.M. Wang, and Y.Q. Fu, Microfluidics and Nanofluidics **18**, 537 (2015).
[236] Y.J. Guo, H.B. Lv, Y.F. Li, X.L. He, J. Zhou, J.K. Luo, X.T. Zu, A.J. Walton, and Y.Q. Fu, Journal of Applied Physics **116**, (2014).
[237] H.F. Pang, Y.Q. Fu, L. Garcia-Gancedo, S. Porro, J.K. Luo, F. Placido, J.I.B. Wilson, A.J. Flewitt, W.I. Milne, and X.T. Zu, Microfluidics and Nanofluidics **15**, 377 (2013).
[238] J. Ho, M.K. Tan, D.B. Go, L.Y. Yeo, J.R. Friend, and H.-C. Chang, Anal. Chem. **83**, 3260 (2011).
[239] A. Qi, L.Y. Yeo, and J.R. Friend, Physics of Fluids **20**, 074103 (2008).
[240] A. Rajapaksa, A. Qi, L.Y. Yeo, R. Coppel, and J.R. Friend, Lab Chip **14**, 1858 (2014).
[241] A. Qi, J.R. Friend, L.Y. Yeo, D.A.V. Morton, M.P. McIntosh, and L. Spiccia, Lab Chip **9**, 2184 (2009).
[242] P.C.L. Kwok, A. McDonnell, P. Tang, C. Knight, E. McKay, S.P. Butler, A. Sivarajah, R. Quinn, L. Fincher, E. Browne, L.Y. Yeo, and H.-K. Chan, International Journal of Pharmaceutics **580**, 119196 (2020).

[243] K.M. Ang, L.Y. Yeo, Y.M. Hung, and M.K. Tan, Lab Chip **16**, 3503 (2016).
[244] K.M. Ang, L.Y. Yeo, J.R. Friend, Y.M. Hung, and M.K. Tan, Journal of Aerosol Science **79**, 48 (2015).
[245] C. Westerhausen, L.G. Schnitzler, D. Wendel, R. Krzysztoń, U. Lächelt, E. Wagner, J.O. Rädler, and A. Wixforth, Micromachines (Basel) **7**, (2016).
[246] A.M. Gracioso Martins, N.R. Glass, S. Harrison, A.R. Rezk, N.A. Porter, P.D. Carpenter, J. Du Plessis, J.R. Friend, and L.Y. Yeo, Anal. Chem. **86**, 10812 (2014).
[247] G. Greco, M. Agostini, R. Shilton, M. Travagliati, G. Signore, and M. Cecchini, Sensors (Basel) **17**, (2017).
[248] R.J. Shilton, L.Y. Yeo, and J.R. Friend, Sensors and Actuators B: Chemical **160**, 1565 (2011).
[249] H. Ahmed, J. Park, G. Destgeer, M. Afzal, and H.J. Sung, Appl. Phys. Lett. **114**, 043702 (2019).
[250] T.-T. Wu and I.-H. Chang, Journal of Applied Physics **98**, 024903 (2005).
[251] J.K. Luo, Y.Q. Fu, Y. Li, X.Y. Du, A.J. Flewitt, A.J. Walton, and W.I. Milne, Journal of Micromechanics and Microengineering **19**, 054001 (2009).
[252] Q. Zeng, F. Guo, L. Yao, H.W. Zhu, L. Zheng, Z.X. Guo, W. Liu, Y. Chen, S.S. Guo, and X.Z. Zhao, Sensors and Actuators B: Chemical **160**, 1552 (2011).
[253] D. Ahmed, X. Mao, J. Shi, B.K. Juluri, and T.J. Huang, Lab Chip **9**, 2738 (2009).
[254] D. Ahmed, C.Y. Chan, S.-C.S. Lin, H.S. Muddana, N. Nama, S.J. Benkovic, and T.J. Huang, Lab Chip **13**, 328 (2013).
[255] S. Orbay, A. Ozcelik, J. Lata, M. Kaynak, M. Wu, and T.J. Huang, J Micromech Microeng **27**, 015008 (2017).
[256] A. Ozcelik, D. Ahmed, Y. Xie, N. Nama, Z. Qu, A.A. Nawaz, and T.J. Huang, Anal. Chem. **86**, 5083 (2014).
[257] N.F. Läubli, M.S. Gerlt, A. Wüthrich, R.T.M. Lewis, N. Shamsudhin, U. Kutay, D. Ahmed, J. Dual, and B.J. Nelson, Anal. Chem. **93**, 9760 (2021).
[258] M. Ovchinnikov, J. Zhou, and S. Yalamanchili, The Journal of the Acoustical Society of America **136**, 22 (2014).
[259] S.A. Endaylalu and W.-H. Tien, Biomicrofluidics **15**, 034102 (2021).
[260] A. Doinikov, M. Gerlt, A. Pavlic, and J. Dual, Microfluidics and Nanofluidics **24**, 32 (2020).
[261] N. Nama, P.-H. Huang, T.J. Huang, and F. Costanzo, Biomicrofluidics **10**, 024124 (2016).
[262] N. Nama, P.-H. Huang, T.J. Huang, and F. Costanzo, Lab Chip **14**, 2824 (2014).
[263] C. Zhang, X. Guo, P. Brunet, M. Costalonga, and L. Royon, Microfluid Nanofluid **23**, 104 (2019).
[264] J. Boss and W. Poland, Bulk Solids Handl **6**, 1207 (1986).
[265] P.-H. Huang, Y. Xie, D. Ahmed, J. Rufo, N. Nama, Y. Chen, C.Y. Chan, and T.J. Huang, Lab on a Chip **13**, 3847 (2013).
[266] C. Zhang, X. Guo, L. Royon, and P. Brunet, Phys Rev E **102**, 043110 (2020).
[267] S. Zhao, W. He, Z. Ma, P. Liu, P.-H. Huang, H. Bachman, L. Wang, S. Yang, Z. Tian, Z. Wang, Y. Gu, Z. Xie, and T.J. Huang, Lab Chip **19**, 941 (2019).
[268] Z. Wang, P.-H. Huang, C. Chen, H. Bachman, S. Zhao, S. Yang, and T.J. Huang, Lab Chip **19**, 4021 (2019).
[269] P.-H. Huang, N. Nama, Z. Mao, P. Li, J. Rufo, Y. Chen, Y. Xie, C.-H. Wei, L. Wang, and T.J. Huang, Lab Chip **14**, 4319 (2014).
[270] A. Ozcelik, N. Nama, P.-H. Huang, M. Kaynak, M.R. McReynolds, W. Hanna-Rose, and T.J. Huang, Small **12**, 5120 (2016).
[271] L. Feng, B. Song, D. Zhang, Y. Jiang, and F. Arai, Micromachines (Basel) **9**, 596 (2018).
[272] L. Sun, T. Lehnert, M.A.M. Gijs, and S. Li, Lab Chip **22**, 4224 (2022).
[273] L. Lin, H. Dang, R. Zhu, Y. Liu, and H. You, Micromachines **13**, 1439 (2022).
[274] M. Zhou, D. Gao, Z. Yang, C. Zhou, Y. Tan, W. Wang, and Y. Jiang, Talanta **222**, 121480 (2021).
[275] T. Hayakawa, S. Sakuma, and F. Arai, Microsyst Nanoeng **1**, 1 (2015).
[276] T. Hayakawa, S. Sakuma, T. Fukuhara, Y. Yokoyama, and F. Arai, Micromachines **5**, 681 (2014).
[277] X. Lu, A. Martin, F. Soto, P. Angsantikul, J. Li, C. Chen, Y. Liang, J. Hu, L. Zhang, and J. Wang, Advanced Materials Technologies **4**, 1800374 (2019).

[278] H. Shen, K. Zhao, Z. Wang, X. Xu, J. Lu, W. Liu, and X. Lu, Micromachines **10**, 882 (2019).
[279] J. Nam and C.S. Lim, Sensors and Actuators B: Chemical **255**, 3434 (2018).
[280] J. Nam, W.S. Jang, and C.S. Lim, Sensors and Actuators B: Chemical **258**, 991 (2018).
[281] M.S. Brugger, K. Baumgartner, S.C.F. Mauritz, S.C. Gerlach, F. Röder, C. Schlosser, R. Fluhrer, A. Wixforth, and C. Westerhausen, Proc Natl Acad Sci USA **117**, 31603 (2020).
[282] D. Liao, F. Li, D. Lu, and P. Zhong, Biochemical and Biophysical Research Communications **518**, 541 (2019).
[283] S. Ramesan, A.R. Rezk, P.M. Cevaal, C. Cortez-Jugo, J. Symons, and L.Y. Yeo, ACS Appl. Bio Mater. **4**, 2781 (2021).
[284] M. Wu, C. Chen, Z. Wang, H. Bachman, Y. Ouyang, P.-H. Huang, Y. Sadovsky, and T. Jun Huang, Lab on a Chip **19**, 1174 (2019).
[285] Z. Wang, H. Wang, R. Becker, J. Rufo, S. Yang, B.E. Mace, M. Wu, J. Zou, D.T. Laskowitz, and T.J. Huang, Microsyst Nanoeng **7**, 1 (2021).
[286] P. Li, Z. Mao, Z. Peng, L. Zhou, Y. Chen, P.-H. Huang, C.I. Truica, J.J. Drabick, W.S. El-Deiry, M. Dao, S. Suresh, and T.J. Huang, Proc Natl Acad Sci U S A **112**, 4970 (2015).
[287] R. Altay, M.K. Yapici, and A. Koşar, Biosensors **12**, 171 (2022).
[288] K. Wang, W. Zhou, Z. Lin, F. Cai, F. Li, J. Wu, L. Meng, L. Niu, and H. Zheng, Sensors and Actuators, B: Chemical **258**, 1174 (2018).
[289] J.W. Ng, C. Devendran, and A. Neild, Lab Chip **17**, (2017).
[290] D.J. Collins, Z. Ma, and Y. Ai, Anal. Chem. **88**, 5513 (2016).
[291] D.J. Collins, B.L. Khoo, Z. Ma, A. Winkler, R. Weser, H. Schmidt, J. Han, and Y. Ai, Lab Chip **17**, 1769 (2017).
[292] Y. Zhou, Z. Ma, and Y. Ai, RSC Adv. **9**, 31186 (2019).
[293] N.R. Glass, R.J. Shilton, P.P.Y. Chan, J.R. Friend, and L.Y. Yeo, Small **8**, 1881 (2012).
[294] M.K. Tan, A. Siddiqi, and L.Y. Yeo, Sci Rep **7**, (2017).
[295] Y. Wang, H. Pan, D. Mei, C. Xu, and W. Weng, Lab Chip **22**, 1149 (2022).
[296] H. Zhu, P. Zhang, Z. Zhong, J. Xia, J. Rich, J. Mai, X. Su, Z. Tian, H. Bachman, J. Rufo, Y. Gu, P. Kang, K. Chakrabarty, T.P. Witelski, and T.J. Huang, Science Advances **7**, eabc7885 (2021).
[297] J. Li, A. Crivoi, X. Peng, L. Shen, Y. Pu, Z. Fan, and S.A. Cummer, Commun Phys **4**, 1 (2021).
[298] J. Park, G. Destgeer, M. Afzal, and H.J. Sung, Lab Chip **20**, 3922 (2020).
[299] V. Bussiere, A. Vigne, A. Link, J. McGrath, A. Srivastav, J.-C. Baret, and T. Franke, Anal. Chem. **91**, 13978 (2019).
[300] A. Link, J.S. McGrath, M. Zaimagaoglu, and T. Franke, Lab Chip **22**, 193 (2022).
[301] P. Zhang, W. Wang, H. Fu, J. Rich, X. Su, H. Bachman, J. Xia, J. Zhang, S. Zhao, J. Zhou, and T.J. Huang, Lab Chip **20**, 4466 (2020).
[302] N. Zhang, A. Horesh, and J. Friend, Advanced Science **8**, 2100408 (2021).
[303] M. Miansari and J.R. Friend, Advanced Functional Materials **26**, 7861 (2016).
[304] C. Bai, C. Wang, T. Zheng, and Q. Hu, CrystEngComm **20**, 1245 (2018).
[305] J.-C. Hsu and Y.-D. Lin, Sensors and Actuators A: Physical **300**, 111651 (2019).
[306] G. Celik Cogal, P.K. Das, G. Yurdabak Karaca, V.R. Bhethanabotla, and A. Uygun Oksuz, ACS Appl. Bio Mater. **4**, 7932 (2021).
[307] L. Ren, S. Yang, P. Zhang, Z. Qu, Z. Mao, P.-H. Huang, Y. Chen, M. Wu, L. Wang, P. Li, and T.J. Huang, Small **14**, 1801996 (2018).
[308] D.J. Collins, B. Morahan, J. Garcia-Bustos, C. Doerig, M. Plebanski, and A. Neild, Nat Commun **6**, 8686 (2015).
[309] C. Xu, C. Wang, T. Zheng, Q. Hu, and C. Bai, CrystEngComm **20**, 7275 (2018).
[310] Z. Tengfei, W. Chaohui, M. Baogang, and J. Zhuangde, CrystEngComm **18**, 6784 (2016).
[311] G. Greco, M. Agostini, I. Tonazzini, D. Sallemi, S. Barone, and M. Cecchini, Anal. Chem. **90**, 7450 (2018).
[312] S. Sreejith, R. Kishor, A. Abbas, R. Thomas, T. Yeo, V.D. Ranjan, R. Vaidyanathan, Y.P. Seah, B. Xing, Z. Wang, L. Zeng, Y. Zheng, and C.T. Lim, ACS Applied Materials & Interfaces (2019).

[313] Y. Lei, H. Hu, J. Chen, and P. Zhang, Actuators **9**, 5 (2020).
[314] D. Sun, K. F. Böhringer, M. Sorensen, E. Nilsson, J. Scott Edgar, and D. R. Goodlett, Lab on a Chip **20**, 3269 (2020).
[315] F. Wu, M.H. Shen, J. Yang, H. Wang, R. Mikhaylov, A. Clayton, X. Qin, C. Sun, Z. Xie, M. Cai, J. Wei, D. Liang, F. Yuan, Z. Wu, Y.Q. (Richard) Fu, Z. Yang, X. Sun, L. Tian, and X. Yang, IEEE Electron Device Letters **PP**, 1 (2021).
[316] J. Nam, H. Lim, C. Kim, J. Yoon Kang, and S. Shin, Biomicrofluidics **6**, 024120 (2012).
[317] X. Ding, S.-C.S. Lin, M.I. Lapsley, S. Li, X. Guo, C.Y. Chan, I.-K. Chiang, L. Wang, J.P. McCoy, and T.J. Huang, Lab Chip **12**, 4228 (2012).
[318] A. Shamloo and M. Boodaghi, Ultrasonics **84**, 234 (2018).
[319] S. Li, X. Ding, Z. Mao, Y. Chen, N. Nama, F. Guo, P. Li, L. Wang, C.E. Cameron, and T.J. Huang, Lab Chip **15**, 331 (2015).
[320] M. Wu, Y. Ouyang, Z. Wang, R. Zhang, P.-H. Huang, C. Chen, H. Li, P. Li, D. Quinn, M. Dao, S. Suresh, Y. Sadovsky, and T.J. Huang, Proc Natl Acad Sci U S A **114**, 10584 (2017).
[321] M.C. Jo and R. Guldiken, Sensors and Actuators A: Physical **207**, 39 (2014).
[322] G. Simon, M.A.B. Andrade, J. Reboud, J. Marques-Hueso, M.P.Y. Desmulliez, J.M. Cooper, M.O. Riehle, and A.L. Bernassau, Biomicrofluidics **11**, 054115 (2017).
[323] J. Lee, C. Rhyou, B. Kang, and H. Lee, J. Phys. D: Appl. Phys. **50**, 165401 (2017).
[324] C. Mu, Z. Zhang, M. Lin, Z. Dai, and X. Cao, Sensors and Actuators B: Chemical **215**, 77 (2015).
[325] M.C. Jo and R. Guldiken, in *2011 Annual International Conference of the IEEE Engineering in Medicine and Biology Society* (2011), pp. 7691–7694.
[326] M.C. Jo and R. Guldiken, Sensors and Actuators A: Physical **187**, 22 (2012).
[327] J.-C. Hsu, C.-H. Hsu, and Y.-W. Huang, Micromachines **10**, 52 (2019).
[328] D.J. Collins, C. Devendran, Z. Ma, J.W. Ng, A. Neild, and Y. Ai, Sci Adv **2**, e1600089 (2016).
[329] G. Feng, L. Peng, B.F. Jarrod, M. Zhangming, Z. Hong, L. Sixing, N. Nitesh, R.F. James, J.B. Stephen, and H. Tony Jun, Proceedings of the National Academy of Sciences **112**, 43 (2015).
[330] C. Devendran, N.R. Gunasekara, D.J. Collins, and A. Neild, RSC Adv. **6**, 5856 (2016).
[331] T. Zheng, C. Wang, C. Xu, Q. Hu, and S. Wei, Sensors and Actuators A: Physical **284**, 168 (2018).
[332] S. Yang, Z. Tian, Z. Wang, J. Rufo, P. Li, J. Mai, J. Xia, H. Bachman, P.-H. Huang, M. Wu, C. Chen, L.P. Lee, and T.J. Huang, Nat. Mater. **21**, 540 (2022).
[333] S.M. Naseer, A. Manbachi, M. Samandari, P. Walch, Y. Gao, Y.S. Zhang, F. Davoudi, W. Wang, K. Abrinia, J.M. Cooper, A. Khademhosseini, and S.R. Shin, Biofabrication **9**, 015020 (2017).
[334] T.D. Nguyen, V.T. Tran, Y.Q. Fu, and H. Du, Appl. Phys. Lett. **112**, 213507 (2018).
[335] B. Chen, Y. Wu, Z. Ao, H. Cai, A. Nunez, Y. Liu, J. Foley, K. Nephew, X. Lu, and F. Guo, Lab Chip **19**, 1755 (2019).
[336] K. Chen, M. Wu, F. Guo, P. Li, C.Y. Chan, Z. Mao, S. Li, L. Ren, R. Zhang, and T.J. Huang, Lab Chip **16**, 2636 (2016).
[337] X. Tao, T.D. Nguyen, H. Jin, R. Tao, J. Luo, X. Yang, H. Torun, J. Zhou, S. Huang, L. Shi, D. Gibson, M. Cooke, H. Du, S. Dong, J. Luo, and Y. Fu, Sensors and Actuators B: Chemical **299**, (2019).
[338] F. Guo, Z. Mao, Y. Chen, Z. Xie, J.P. Lata, P. Li, L. Ren, J. Liu, J. Yang, M. Dao, S. Suresh, and T.J. Huang, PNAS **113**, 1522 (2016).
[339] I. Bernard, A.A. Doinikov, P. Marmottant, D. Rabaud, C. Poulain, and P. Thibault, Lab Chip **17**, 2470 (2017).
[340] M.C. Jo and R. Guldiken, Sensors and Actuators A: Physical **196**, 1 (2013).
[341] Y. Sriphutkiat and Y. Zhou, Sensors **17**, 106 (2017).
[342] A. Zhang and Y. Zha, J Sep Sci **36**, 1085 (2013).
[343] A.-L. Zhang and Y. Zha, Chemical Engineering and Processing: Process Intensification **62**, 145 (2012).
[344] G. Destgeer and H.J. Sung, Lab Chip **15**, 2722 (2015).
[345] A.G. Guex, N. Di Marzio, D. Eglin, M. Alini, and T. Serra, Materials Today Bio **10**, 100110 (2021).
[346] Y. Li, S. Cai, H. Shen, Y. Chen, Z. Ge, and W. Yang, Biomicrofluidics **16**, 031502 (2022).

[347] J. Mei, A. Vasan, U. Magaram, K. Takemura, S.H. Chalasani, and J. Friend, Biomed Microdevices **24**, 18 (2022).
[348] P. Liu, Z. Tian, N. Hao, H. Bachman, P. Zhang, J. Hu, and T.J. Huang, Lab Chip **20**, 3399 (2020).
[349] T. Peng, L. Li, M. Zhou, and F. Jiang, Sensors **22**, 1269 (2022).
[350] H. Bachman, Y. Gu, J. Rufo, S. Yang, Z. Tian, P.-H. Huang, L. Yu, and T.J. Huang, Lab Chip **20**, 1281 (2020).
[351] P. Liu, Z. Tian, K. Yang, T.D. Naquin, N. Hao, H. Huang, J. Chen, Q. Ma, H. Bachman, P. Zhang, X. Xu, J. Hu, and T.J. Huang, Science Advances **8**, eabm2592 (2022).